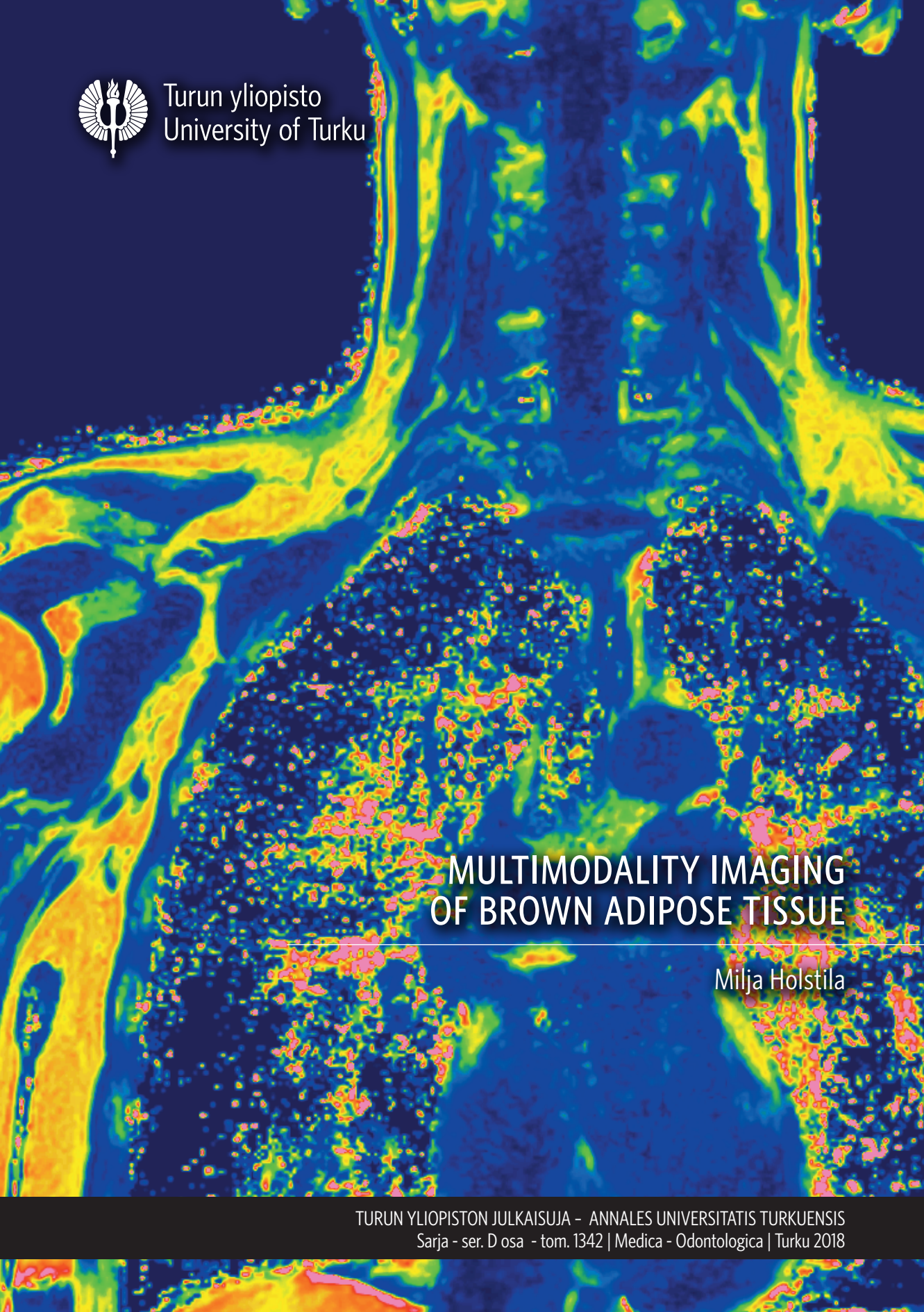

Turun yliopisto
University of Turku

MULTIMODALITY IMAGING OF BROWN ADIPOSE TISSUE

Milja Holstila

TURUN YLIOPISTON JULKAISUJA – ANNALES UNIVERSITATIS TURKUENSIS
Sarja - ser. D osa - tom. 1342 | Medica - Odontologica | Turku 2018

Turun yliopisto
University of Turku

MULTIMODALITY IMAGING OF BROWN ADIPOSE TISSUE

Milja Holstila

TURUN YLIOPISTON JULKAISUJA – ANNALES UNIVERSITATIS TURKUENSIS
Sarja - ser. D osa - tom. 1342 | Medica - Odontologica | Turku 2018

University of Turku

Faculty of Medicine
Department of Radiology
Doctoral Programme in Clinical Research
Turku PET Centre
Medical Imaging Centre of Southwest Finland, Turku University Hospital

Supervised by

Professor Riitta Parkkola
Turku PET Centre
Department of Radiology
Turku University Hospital and
University of Turku, Turku, Finland

Professor Pirjo Nuutila
Turku PET Centre
Department of Endocrinology
Turku University Hospital and
University of Turku, Turku, Finland

Associate Professor Ronald J.H. Borra
Department of Nuclear Medicine and
Molecular Imaging
University Medical Center Groningen and
University of Groningen,
Groningen, The Netherlands

Reviewed by

Assistant Professor Vera Schrauwen-Hinderling
Department of Radiology
Maastricht University Medical Centre and
University of Maastricht,
Maastricht, The Netherlands

Opponent

Professor Osmo Tervonen
Department of Radiology
Oulu University Hospital and
University of Oulu, Oulu, Finland

Cover image by Milja Holstila and Mira Hallenberg

ISBN 978-951-29-7187-9 (PRINT)
ISBN 978-951-29-7188-6 (PDF)
ISSN 0355-9483 (Print)
ISSN 2343-3213 (Online)
Painosalama Oy – Turku, Finland 2018

"See your world through my eyes:
A universe so vast as to be immeasurable
– incomprehensible even to your greatest minds."

Algalon

ABSTRACT

Milja Holstila

MULTIMODALITY IMAGING OF BROWN ADIPOSE TISSUE

University of Turku
Faculty of Medicine
Department of Radiology
Doctoral Programme in Clinical Research
Turku PET Centre
Medical Imaging Centre of Southwest Finland, Turku University Hospital

Annales Universitatis Turkuensis
Painosalama Oy, Turku, Finland 2018

There are two types of adipose tissue in the human body. White adipose tissue (WAT) stores energy, while brown adipose tissue (BAT) consumes it. BAT can be activated by exposure to cold to generate heat. Human adults seem to have recruitable 'beige' or 'brite' fat, which is derived from WAT. The cells can take on the appearance and function of BAT upon prolonged stimulation by cold, but the process can also be reversed. Thus adult human BAT contains a mixture of brown and white adipocytes at different stages, the triglyceride content being a continuous spectrum.

Human BAT is highly insulin-sensitive. Decreases in BAT mass and activity may have a role in the development of obesity and diabetes in adulthood. The prevalence of these conditions is growing worldwide, leading to a global health issue and socioeconomic problem. This poses a great need for rapid and affordable means of studying fat tissue.

The in vivo localization and activation state of BAT has been assessed by ^{18}F-fluorodeoxyglucose positron emission tomography (^{18}FDG-PET/CT), which involves the intravenous injection of radioactive tracer, as well as exposure to radiation by computed tomography. Due to the differences in the tissue structure, water and iron content, magnetic resonance imaging (MRI) can reliably measure BAT volume and water content regardless of the activation state. As a method it is noninvasive, safe and more readily available than ^{18}FDG-PET.

The aim was to develop and test MRI methods for detecting, quantifying and examining BAT. The methods include in-phase and out-of-phase (in/opp) imaging, signal-fat-fraction (SFF) analysis based on the Dixon method, T2* relaxation time mapping and single-voxel proton magnetic resonance spectroscopy (^{1}H MRS). Our results suggest that MRI methods can identify BAT and quantify fat deposit triglyceride content independent of cold-induced BAT activation and without radiation burden. It was also shown that the triglyceride content in supraclavicular fat deposits measured by ^{1}H-MRS may be an independent marker of whole-body insulin sensitivity.

Keywords: brown adipose tissue, BAT, diabetes, obesity, magnetic resonance imaging, MRI, proton magnetic resonance spectroscopy, ^{1}H MRS, positron emission tomography, PET

TIIVISTELMÄ

Milja Holstila

RUSKEAN RASVAKUDOKSEN KUVANTAMINEN ERI KUVANTAMISMENETELMILLÄ

Turun yliopisto
Lääketieteellinen tiedekunta
Radiologian oppiaine
Turun kliininen tohtoriohjelma
Valtakunnallinen PET-keskus
Varsinais-Suomen kuvantamiskeskus, Turun yliopistollinen keskussairaala

Annales Universitatis Turkuensis
Painosalama Oy, Turku, Suomi 2018

Ihmiskehossa on kahdenlaista rasvakudosta. Valkoinen rasva (WAT) varastoi energiaa, ruskea rasva (BAT) kuluttaa sitä. Kylmäaltistus voi aktivoida ruskean rasvan tuottamaan lämpöä. Aikuisilla on hankinnaista "beige" tai "brite" -rasvaa, joka on muuntunutta valkoista rasvaa. Pitkittyneessä kylmäaltistuksessa WAT-solut voivat ulkonäöltään ja toiminnaltaan muuntua BAT-solujen kaltaisiksi, mutta tapahtumasarja voi kulkea myös toiseen suuntaan. Aikuisella ihmisellä BAT on siis sekoitus eri asteisesti kypsyneitä ruskeita ja valkoisia rasvasoluja, joiden triglyseridipitoisuus muuttuu liukuvasti.

Ihmisellä BAT on vahvasti insuliiniherkkää. BAT:n määrän ja aktiivisuuden vähentymisellä voi olla merkitystä lihavuudessa ja aikuisiän diabeteksessa. Näiden esiintyminen on globaalisti kasvussa, mikä johtaa maailmanlaajuisiin terveysongelmiin ja sosioekonomisiin ongelmiin. On siis tarvetta nopeille ja edullisille tavoille tutkia rasvakudosta.

BAT:n sijaintia ja aktivoitumista on tutkittu ^{18}F-fluorodeoksiglukoosipositroniemissio-tomografialla (^{18}FDG-PET/CT), jossa aiheutuu sädealtistus suonensisäisestä radioaktiivisesta merkkiaineesta ja tietokonetomografiakuvauksesta. Kudoksen rakenne-eroista sekä vesi- ja rautapitoisuudesta johtuen magneettiresonanssikuvantaminen (MRI) mittaa luotettavasti BAT:n tilavuutta ja vesipitoisuutta. Menetelmänä se on kajoamaton, turvallinen ja helpommin saatavissa kuin PET.

Tavoitteena oli kehittää ja testata MRI-menetelmiä ruskean rasvan toteamiseen, mittaamiseen ja arviointiin. Menetelminä olivat in-phase/out-of-phase (in/opp) -kuvantaminen, dixon-menetelmään perustuva signaalirasvasuhdekuvantaminen (SFF), T2*-relaksaatioaikakartoitus sekä yksittäisen vokselin protonimagneettispektroskopia (^{1}H MRS). Tuloksiemme mukaan MRI-menetelmät pystyvät arvioimaan rasvan triglyseridipitoisuutta kylmäaktivaatiosta riippumatta ja ilman säderasitusta. Osoitimme myös, että solisluun alapuolisen BAT-kertymän triglyseridipitoisuus voi olla kehon insuliiniherkkyyden itsenäinen merkkitekijä.

Avainsanat: ruskea rasvakudos, BAT, diabetes, lihavuus, magneettikuvaus, MRI, protonimagneettispektroskopia, ^{1}H MRS, positroniemissiotomografia, PET

TABLE OF CONTENTS

ABBREVIATIONS

ATP	Adenosine Triphosphate
B_0	Magnetic Field (Static)
BAT	Brown Adipose Tissue
BMI	Body Mass Index
BOLD	Blood-oxygen-level Dependent
CO_2	Carbon Dioxide
CT	Computed Tomography
DWI	Diffusion Weighted Imaging
ECG	Electrocardiogram
FA	Flip Angle
^{18}FDG	[^{18}F]-2-fluoro-2-deoxy-D-glucose
^{18}FTHA	[^{18}F]-fluoro-6-thia-heptadecanoic acid
FFA	Free Fatty Acid
FFE	Fast Field Echo
fMRI	Functional Magnetic Resonance Imaging
FOV	Field of View
^{1}H MRS	Proton Magnetic Resonance Spectroscopy
HDL	High Density Lipoprotein
HU	Hounsfield Unit
IDF	International Diabetes Federation
in/opp	In-phase and Out-of-phase
IRT	Infrared Thermography
LDL	Low Density Lipoprotein
M_0	Net Magnetization
MR	Magnetic Resonance
MRI	Magnetic Resonance Imaging
MRS	Magnetic Resonance Spectroscopy
NMR	Nuclear Magnetic Resonance
NMV	Net Magnetization Vector
OGTT	Oral Glucose Tolerance Test
^{15}O H_2O	[^{15}O]-water
PET	Positron Emission Tomography
PET/CT	Positron Emission Tomography combined with Computed Tomography
PET/MRI	Positron Emission Tomography combined with Magnetic Resonance Imaging
RF	Radio Frequency
ROI	Region of Interest

SD	Standard Deviation
SFF	Signal-Fat-Fraction
SI	Signal Intensity
SPIR	Spectral Presaturation with Inversion Recovery
SUV	Standard Uptake Value
T	Tesla
T1	Spin-lattice (longitudinal) relaxation time
T2	Spin-spin (transverse) relaxation time
T2*	Effective spin-spin (transverse) relaxation time
T2DM	Type 2 Diabetes Mellitus
TE	Echo Time
TR	Time of Repetition
UCP-1	Uncoupling Protein 1
US	Ultrasonography
VOI	Volume of Interest
WAT	White Adipose Tissue
WHO	World Health Organization

LIST OF ORIGINAL PUBLICATIONS

This thesis is based on the following original publications, which are referred to in the text by roman numerals I-III.

I Holstila M, Virtanen KA, Grönroos TJ, Laine J, Lepomäki V, Saunavaara J, Lisinen I, Komu M, Hannukainen JC, Nuutila P, Parkkola R, Borra RJH. Measurement of Brown Adipose Tissue Mass using a Novel Dual-Echo MR Imaging Approach: a Validation Study. Metabolism. 2013 Aug;62(8):1189-98.

II Raiko J*, Holstila M*, Virtanen KA, Orava J, Saunavaara V, Niemi T, Laine J, Taittonen M, Borra RJH, Nuutila P, Parkkola R. Brown Adipose Tissue Triglyceride Content is Associated with Decreased Insulin Sensitivity, Independently of Age and Obesity. Diabetes Obes Metab. 2015 May;17(5):516-9.

III Holstila M, Pesola M, Saari T, Koskensalo K, Raiko J, Borra RJH, Nuutila P, Parkkola R, Virtanen KA. MR Signal-fat-fraction Analysis and T2* Weighted Imaging Measure BAT Reliably on Humans Without Cold Exposure. Metabolism. 2017 May;70(5):23-30.

*These authors contributed equally to this work.

1 INTRODUCTION

Obesity has reached epidemic proportions globally, with at least 2.8 million people dying each year as a result of being overweight or obese (WHO 2013). Once associated with high-income countries, obesity is now also prevalent in low- and middle-income countries. The tremendous rise in the incidence of type 2 (T2DM) diabetes has been attributed to the worldwide increase in obesity, resulting from excess calorie intake and lack of physical exercise (WHO 2016).

Obesity is a major risk factor for also other noncommunicable diseases such as cardiovascular diseases, musculoskeletal disorders such as osteoarthritis, and some cancers, including endometrial, breast, ovarian, prostate, liver, gallbladder, kidney, and colon cancer. (WHO 2013)

We lack effective treatment and prevention options because we do not fully understand the mechanics of obesity. With increased research across a variety of innovative areas, we may expect to address the impact obesity will have on the public health in the near future. Among other interesting concepts for obesity research, brown adipose tissue (BAT) has been catching the attention of scientists during the last few years.

BAT is specialized fat tissue that burns energy for thermogenesis, as opposed to white adipose tissue (WAT), which stores energy. Until a few years ago, BAT was thought to be functionally important only in small mammals and infants, with negligible physiological relevance in adult humans. Three studies published simultaneously in 2009 unambiguously demonstrated that healthy adult humans have significant depots of metabolically active BAT. (Cypess et al. 2009; van Marken Lichtenbelt et al. 2009; Virtanen et al. 2009)

BAT is prevalent in children, with its activity increasing until adolescence, but after that the prevalence gradually decreases with age (Drubach et al. 2011). Outdoor temperature, age, sex, BMI, and diabetic status have been identified as determinants of the prevalence, mass, and glucose uptake activity of BAT (Ouellet et al. 2011). In adult humans, the amount of BAT is small, and most prominent BAT depots are localized in the supraclavicular areas. Due to brown adipocytes consisting of numerous small lipid droplets instead a sizeable single droplet found in WAT, and a much higher number of iron-containing mitochondria, BAT contains more water and iron as well as less triglycerides than WAT.

To be able to study the metabolic functions of BAT, robust, safe and widely available imaging methods are needed. BAT biopsies would provide confirmation of the tissue cellularity, but this invasive procedure is not a feasible tool for clinical practice. Positron emission tomography (PET) is currently considered the gold standard for

assessing the metabolic activation of BAT. In this technique, short-lived positron-emitting isotopes allow for sensitive and accurate quantification of the metabolic processes of the tissues in vivo. [^{18}F]-2-fluoro-2-deoxy-D-glucose (^{18}FDG) is the most commonly used PET tracer. However, PET scans involve potentially harmful radiation exposure, and their availability is often limited.

Magnetic resonance imaging (MRI) allows for high resolution and good tissue contrast imaging of the fat tissue without the radiation exposure. Specialized techniques such as proton magnetic resonance spectroscopy (^{1}H-MRS), Dixon imaging and T2* mapping make MRI an ideal imaging modality for assessing tissue fat and iron content noninvasively in vivo.

2 REVIEW OF LITERATURE

2.1 ADIPOSE TISSUE

Adipose tissue used to be regarded as connective tissue which stores energy without a specific anatomy. However, accumulating data support the idea of a large adipose organ with a discrete anatomy, specific vascular and nerve supplies, complex cytology, and high physiological plasticity. This organ is distributed in several locations around the body, the main areas being below the skin (subcutaneous depots) and in the trunk (visceral depots). It contributes to several crucial survival needs in a mammal body, including thermogenesis, lactation, immune responses, and fuel for metabolism. (Cinti 2011, 2012)

Adipose tissue is one of the main types of connective tissue. It is composed mostly of adipocytes, but also contains vascular structures and fibroblasts. In recent years, adipose tissue has been recognized as a major endocrine organ, producing hormones such as leptin, estrogen, resistin, and the cytokine TNFα. Adipocytes contain a significant amount of lipids in intracellular lipid droplets. The two types of adipose tissue are WAT, which stores energy, and BAT, which generates body heat. (Cinti 2012)

2.1.1 White adipose tissue

In humans, white adipose tissue is located beneath the skin (subcutaneous fat), around the internal organs (visceral fat), in bone marrow (yellow bone marrow), between the muscles (intermuscular fat) and in female breast tissue. The main role of WAT is to store energy in the form of lipids, although it also cushions and insulates the body, as well as functioning as a major endocrine organ. (Cinti 2012)

Abundant WAT is distributed throughout the entire body and has the capacity to expand massively. Fat mass can vary anywhere from 2–3% of body weight to 60–70% of body weight (Hausman et al. 2001). There is no generally accepted definition of obesity based on total body fat. Most researchers have used >25% in men, and >30% in women, as cut-points to define obesity (Okorodudu et al. 2010).

Obesity results in an ectopic accumulation of fat in WAT, as well as in abnormal locations such as the liver, heart, pancreas and skeletal muscle. Ectopic fat accumulating in the liver and pancreas on patients with T2DM has been shown to be a marker for whole-body insulin resistance (Sattar and Gill 2014).

Visceral fat (intra-abdominal adipose tissue) is located inside the abdominal cavity, packed between the organs. Visceral fat is considered to be more metabolically active than subcutaneous fat (Moller and Kaufman 2005). Excess visceral fat is also linked to T2DM (Montague and O'Rahilly 2000), insulin resistance (Kern et al. 2001),

inflammatory diseases (Marette 2003), and other obesity-related diseases (Mokdad et al. 2003).

The majority of nonvisceral fat is found between the skin and the superficial muscle fascia in the hypodermis. This subcutaneous fat is considered to be less of a health concern than visceral fat (Hamdy, Porramatikul, and Al-Ozairi 2006). Subcutaneous fat is also part of the endocrine system.

2.1.2 Brown adipose tissue

Nowadays it is recognized that humans have two different types of BAT: 'classic BAT' on the infant interscapular area, and 'inducible thermogenic BAT' mainly on the supraclavicular area, manifesting after infancy. The latter is also known as beige or brite fat, and is believed to derive from the same adipogenic lineage as WAT. (Lidell et al. 2013; Wu et al. 2012)

After prolonged or recurrent cold exposure, these inducible BAT cells can change their appearance and function to that of BAT, but the process can also be reversed. That is the reason for adult human BAT containing a mixture of both brown and white adipocytes at different stages of differentiation (Rosenwald et al. 2013), the tissue triglyceride content being a continuous spectrum. This also makes it challenging to define and differentiate BAT from the surrounding tissues. It may be possible that the transformation of inducible BAT back to WAT is part of the same process as ectopic fat accumulation, contributing in metabolic syndrome.

BAT is characterized by a relatively high water and low triglyceride content compared to WAT. Brown adipose cells have high number of intracellular lipid droplets and mitochondria, which contribute to the brownish appearance of the tissue (Cinti 2006). BAT is well-vascularized tissue with a network of blood vessels and noradrenergic nerve endings (Cinti 2009). In addition, BAT exclusively expresses the uncoupling protein-1 (UCP-1) in the mitochondria, which uncouples the cellular respiratory chain, thus allowing for the generation of heat instead of the creation of adenosine triphosphate (ATP) (Inokuma et al. 2005; Jezek and Garlid 1998).

Cold conditions activate BAT, generating a non-shivering thermogenic state (Lee et al. 2010; Saito et al. 2009), as shown in Figure 1. Cold exposure induces sympathetic nervous system activity and BAT metabolism in humans, and seems thus to result in improved glucose metabolism without affecting pancreatic insulin secretion (Iwen et al. 2017).

BAT also responds to stimulation by insulin (Orava et al. 2011), thyroid hormones (Lahesmaa et al. 2014) and glucocorticoid hormones (Scotney et al. 2017). In response to insulin stimulation, glucose uptake in BAT is approximately fivefold compared to fasting conditions. Insulin increases glucose transport into BAT, while

acute cold exposure increases both glucose uptake and perfusion in BAT (Orava et al. 2011). Decreases in the amount and activity of BAT may have a role in the development of obesity and T2DM.

In humans, newborns have the most prevalent BAT, and the amount of the tissue decreases with age (Yoneshiro et al. 2011). In adult humans, active BAT is found in the cervical, supraclavicular, paravertebral, and perirenal areas, with the most prominent BAT depot situated in the supraclavicular area (van Marken Lichtenbelt et al. 2009; Virtanen et al. 2009).

These seem to represent two different types of BAT; infants have 'classical BAT' in the interscapular area, while adults possess 'inducible thermogenic BAT', which is also called beige or brite fat (Lidell et al. 2013; Wu et al. 2012; Cinti 2009). This recruitable beige/brite fat is derived from WAT. The cells may retain high levels of UCP-1 and a multilocular appearance upon prolonged cold exposure, and the process can also be reversed (Rosenwald et al. 2013). In accordance with this, adult human BAT contains a mixture of beige and white adipocytes at different stages (Rosenwald et al. 2013), the triglyceride content being a continuous spectrum. This causes challenges in the definition and differentiation of BAT.

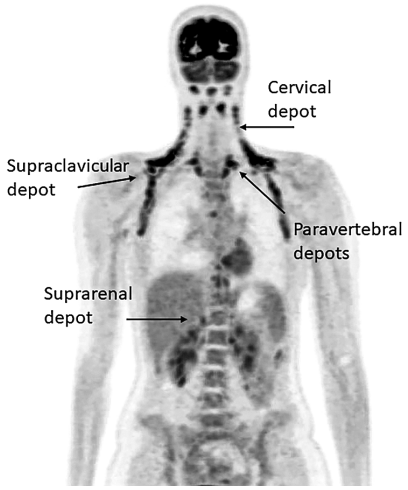

Figure 1. Maximum intensity projection ^{18}FDG-PET image of upper body. In adult humans, active BAT is found in the cervical, supraclavicular, paravertebral, and suprarenal areas.

Reduction in the amount and activation of BAT may have a role in the development of adulthood obesity and diabetes. BAT triglyceride content is lower compared to WAT (Virtanen et al. 2009), and the volume of metabolically active BAT correlates inversely with the amount of body fat (Saito et al. 2009). Brown adipose tissue detected by ^{18}FDG-PET imaging is associated with less central obesity (Green et al. 2017). Human BAT is highly insulin-sensitive (Orava et al. 2011), and BAT metabolic activity measured by ^{18}FDG-PET correlates with whole-body insulin sensitivity (Orava et al. 2013). After stimulation with insulin, the glucose uptake of BAT can be as high as fivefold compared to the fasting state (Orava et al. 2011). Insulin increases glucose

transport into BAT, while acute cold exposure increases both glucose uptake and perfusion in BAT (Orava et al. 2011). BAT volume is significantly associated with increased whole-body lipolysis, triglyceride-free fatty acid (FFA) cycling, FFA oxidation, and adipose tissue insulin sensitivity (Chondronikola et al. 2016).

2.2 OBESITY AND METABOLIC SYNDROME

According to World Health Organization (WHO), obesity is characterized by a BMI (defined as a person's weight in kilograms divided by the square of their height in meters) greater than or equal to 30 kg/m^2 (WHO 2013). In an obese person, the amount of adipose tissue is greatly increased.

The development of obesity represents a state of energy imbalance where energy intake exceeds energy expenditure, leading to the storage of excess energy as fat. The continuous burden of excess energy intake results in hypertrophy of adipose tissue, and often in ectopic fat deposition as well as insulin resistance and metabolic disorders. (Guilherme et al. 2008)

2.2.1 Epidemiology of obesity and metabolic syndrome

Metabolic syndrome is a definition used to describe a cluster of metabolic disorders including insulin resistance, alterations in glucose and lipid metabolism, increased blood pressure, and visceral obesity. Each of the components increases the cardiovascular risk, but the combination of factors is more important. Insulin resistance is the factor most frequently associated with the singular components of the syndrome. (Moller and Kaufman 2005)

However, visceral obesity seems to be the main driving factor due to the increased production of free fatty acids, which seems to interfere with the action of insulin. Weight gain and obesity has been shown to be a strong predictor of metabolic syndrome. Interventions to treat visceral obesity by means of losing weight seem to be the most efficacious way to treat metabolic syndrome, thus improving the most widespread cardiovascular risk factor in western countries. (Bosello and Zamboni 2000)

Global estimates by the World Health Organization indicate that the epidemic of obesity is on the rise worldwide. In 2014, 39% of adults worldwide aged 18 years and older (38% of men and 40% of women) were overweight, defined as body mass index (BMI) ≥ 25). Between 1980 and 2014, the worldwide prevalence of obesity nearly doubled, with 11% of men and 15% of women being classified as obese. In 2013, an estimated 42 million children aged under 5 years (6.3%) were overweight, an increase from around 5% in 2000 to 6% in 2010 and 6.3% in 2013, with the highest rates of increase being observed in Africa and Asia. Diabetes was directly responsible for 1.5 million deaths in 2012. (WHO 2016)

2.2.2 Etiology and epidemiology of diabetes

Diabetes mellitus is a metabolic disorder characterized by elevated blood glucose levels. The majority of diabetes cases (about 90%) are T2DM, with the other 10% being diabetes mellitus type 1 and gestational diabetes (IDF 2015). Diabetes is diagnosed by laboratory tests such as fasting plasma glucose, oral glucose tolerance test, or HbA1C. In the oral glucose tolerance test, plasma glucose is determined after fasting and then 2 hours after ingestion of 75 grams of glucose. Glycated hemoglobin (HbA1C) is a form of hemoglobin that is measured primarily to identify the three-month average plasma glucose concentration, with higher values indicating poorer control of blood glucose levels. (WHO 2016)

T2DM is a chronic disease characterized by hyperglycemia, insulin resistance, and relative lack of insulin. Insulin is secreted by beta cells located in the pancreatic islets of the pancreas. The dysfunction and decrease in mass of pancreatic beta cell are an essential part of T2DM pathogenesis, limiting the beta cell compensation of insulin resistance (Cernea and Dobreanu 2013).

Long-term complications from elevated blood glucose levels include macrovascular complications (atherosclerosis leading to coronary heart disease, cerebrovascular disease, and peripheral arterial disease) and microvascular complications (diabetic retinopathy, nephropathy, and neuropathy) (Konig et al. 2013). T2DM primarily occurs as a result of obesity and a sedentary lifestyle (Hamilton, Hamilton, and Zderic 2014). Thus T2DM is partly preventable by adhering to the guidelines for normal body weight, recommended physical activity and a healthy diet. Treatment involves exercise and dietary changes (Colberg et al. 2010). If the lifestyle interventions are not adequate to normalize the blood sugar levels, oral medication is prescribed.

Rates of T2DM have increased markedly in recent years in parallel with obesity. According to the International Diabetes Federation (IDF), the worldwide prevalence of diabetes mellitus in 2011 was 366 million and will increase to 439 million adults (or 7.7% comparative prevalence) by 2030. In addition, in 2011, the worldwide prevalence of impaired glucose tolerance, widely recognized as a marker of pancreatic beta cell dysfunction and insulin resistance, and as such a precursor to diabetes mellitus, was estimated at 280 million with projections to reach 398 million by 2030 (Shaw, Sicree, and Zimmet 2010).

Diabetes imposes a large economic burden on health care systems across the world, yet varies across world regions. The prevention and effective management of diabetes should be a public health priority to reduce the financial burden (da Rocha et al. 2016). Conceivably, BAT could be a target for obesity management in the future (Loh, Kingwell, and Carey 2017).

2.3 ASSESSMENT OF BROWN ADIPOSE TISSUE

2.3.1 Positron Emission Tomography

Positron emission tomography (PET) is a computerized functional imaging technique utilizing short-lived nuclear medicine radioactive isotopes. In brief, PET is based on detecting a positron-emitting radionuclide tracer introduced into the body on a biologically active molecule. The emitted positron combines with a local electron in the tissue in a process called annihilation, in which two high-energy photons depart in opposite directions. The photons (coincidence events) are detected by the PET scanner. Three-dimensional images of tracer concentration within the body are then constructed using computer analysis. (Das 2015)

PET metabolic imaging has two primary acquisition modalities. Whole-body static scanning is the more commonly used of the techniques. It excels at the anatomical detection of normal and pathological structures and at the determination of the relative uptake of the PET tracer, expressed as standard uptake value (SUV). Static scanning is typically used with tracers displaying delayed tissue metabolic clearance, such as ^{18}FDG or [^{18}F]-fluoro-6-thia-heptadecanoic acid (^{18}FTHA), allowing the comparison of the cumulative tracer uptake between different tissues throughout the whole body. It is able to measure the relative integrated uptake of the tracer between tissues, but cannot precisely determine quantitative fluxes of the tracer in and out of the tissues. Dynamic acquisition PET scanning measures the flux of the tracer in and out of tissues directly. It is more challenging to perform, requiring relatively long acquisition scans targeted at a limited anatomical area determined by the field of view of the scanner, the determination of availability of the tracer in the arterial blood to the tissues of interest, and if the tracer is metabolized, measurements of the metabolite fraction over time using repeated blood samples. The modelization of the data should be performed using linearization compartmental modeling or spectral analysis. (Karakatsanis et al. 2013)

PET as an imaging modality is conveying primarily functional information, dealing with biochemistry and metabolic changes that occur at the molecular level. It allows for quantitative measurements of the regional substrate metabolism. The molecular sensitivity of PET is impressive, reaching the picomolar range and thus permitting the use of minuscule doses of tracers while retaining high specific activity. Usually a PET scanner is combined with either a computed tomography (CT) or magnetic resonance (MR) scanner, for attenuation correction and to provide a good quality anatomical reference.

2.3.1.1 ^{18}FDG-PET

The molecule most commonly used in PET imaging is fluorine labeled glucose ([^{18}F]-2-fluoro-2-deoxy-D-glucose, ^{18}FDG). The tracer indicates the amount of glucose

metabolism, and reduced or increased, it can provide information on a wide range of physiological and pathological phenomena. (Das 2015)

^{18}FDG is administered as an intravenous bolus. It is transported from the bloodstream across the cell membrane to the cells in relation to glucose metabolism. ^{18}FDG accumulates intracellularly, because the flow out of the cell is very slow due to phosphorylation. It remains trapped in the cell in the form of 6-phosphate-fluoro-deoxyglucose because it cannot be metabolized through the glycolytic pathway (Sokoloff et al. 1977). This process contributes to an accumulation of the tracer in the target area, promoting specific and sensitive imaging.

When no cold exposure or hormonal stimulus are present, BAT glucose metabolism does not considerably differ from that of WAT (Orava et al. 2011). While activated, BAT has higher glucose metabolism, due to the high number of intracellular mitochondria and high energy consumption. As a result, functional metabolically active BAT can be investigated using ^{18}FDG-PET. It is excellent at evaluating the activation state of BAT, but volume measurements based on PET activation are not reliable, due to the spillover effect, described as the contamination of activity from neighboring tissues caused by the limited spatial resolution (Croteau et al. 2010). In addition, since adult BAT is a mixture of brown and white adipose cells at different stages of differentiation, a technique for quantifying the triglyceride content of the tissue would generate important additional information. A complementary and reliable method for anatomical and volume measurements is thus needed.

^{18}FDG-PET combined with CT (^{18}FDG-PET/CT) examination has until recently been the gold standard for the assessment of BAT. This procedure is, however, associated with low availability, high costs and above all a significant amount of radiation (Quinn et al. 2016). Even if there has been a reduction in the radiation doses due to low-dose protocols and iterative reconstruction (Willowson, Bailey, and Bailey 2012), the repeated examinations needed to fully evaluate and understand BAT in different circumstances quickly accumulate the radiation burden. (Chen et al. 2016)

In summary, ^{18}FDG-PET/CT is a suboptimal method for the assessment of BAT for research purposes in the population of mainly healthy volunteers, especially when repeated examinations are needed. Therefore, there has been a highly increasing focus on finding safe and easily available methods for assessing BAT volume and triglyceride content.

2.3.1.2 ^{15}O-H_2O perfusion

Perfusion is defined to be the volume of blood flowing through a certain mass (or volume) of tissue per unit time. Tissue perfusion can be measured noninvasively using several imaging methods, including computed tomography, MR perfusion

imaging and PET. Of those, the gold standard is PET with radiowater (^{15}O-H_2O), which is diffusible and inert, exchanging freely between blood and tissues (Sharp 1994). BAT can be detected using perfusion imaging due to the increased blood flow of the tissue during cold activation. In ambient conditions, BAT blood flow is only slightly higher than that of WAT (Din et al. 2016).

2.3.2 MR Imaging and Spectroscopy

MRI is considered to be the best noninvasive imaging method for studying fat tissue due to its supreme soft tissue contrast, spatial resolution, and nonionizing nature (Hu et al. 2012). The technique is very versatile, with different sequences and applications. The development of this modality in the recent decades of radiology has been phenomenal.

The concept of MR imaging was independently discovered by two researchers in 1946, by Felix Bloch (Bloch 1946) and Edward Purcell et al. (Purcell 1945).The alignment of nuclear magnetic moments with the external magnetic field, their precession at Larmor frequency, and the resonance phenomenon enables the transfer of the energy and the change in direction of nuclear net magnetization caused by a radio frequency (RF) pulse. Bloembergen et al. continued the work on the basis of nuclear magnetic resonance (NMR) absorption, creating the concept of T1 and T2 relaxation times (Bloembergen, Purcell, and Pound 1948).

Nuclei with an odd atomic weight (meaning they have odd total number of protons and neutrons) possess a fractional nuclear spin, an intrinsic form of angular momentum. This produces a magnetic field, which is aligned with the axis of rotation of the nucleus. The atom best suited for MR imaging is ^{1}H (proton), due to the odd atomic weight and ubiquity of hydrogen in organic chemistry. Other nuclei besides ^{1}H that are prevalent in a living tissue and can be observed with MRS are ^{13}C, ^{19}F, ^{23}Na and ^{31}P.

2.3.2.1 Physics of magnetic resonance

In normal circumstances, the spins in tissue are randomly oriented, the vectors producing a zero sum when added together. This results in no overall net magnetization. However, when located in an external magnetic field (B_0), in this case produced by the MR scanner, the spins align, either parallel with B_0, or anti-parallel, i.e. 180˚ opposite to it. The spins have a small preference for parallel alignment. The higher the external magnetic field, the larger proportion of the spins will be aligned parallel with B_0 (low energy state) instead of anti-parallel, B_0 (high energy state). This results in the net magnetization (M_0) that differs from zero, oriented in the direction of B_0. (Pooley 2005)

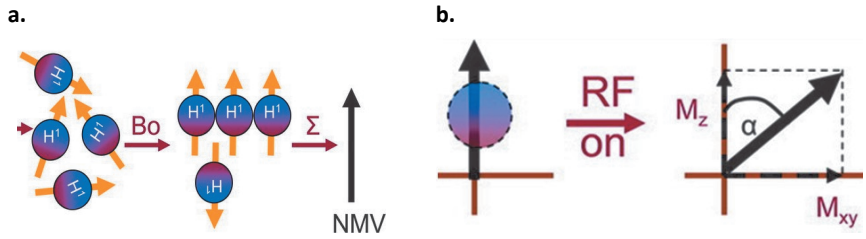

Figure 2. **a)** Initially the magnetic vectors of nuclei are randomly oriented (left), but the nuclear vectors rapidly preferentially align with an external magnetic field (B_0). This causes the sum of these miniature vectors, called the net magnetization vector (NMV), to differ from zero. **b)** The RF pulse changes the orientation of the magnetization of the nuclei and flips the NMV toward the transversal plane. The transversal component of NMV induces a current in the receiver coil and is used for signal creation. M_z = longitudinal magnetization, M_{xy} = transversal magnetization, and α = flip angle. Modified and reprinted with permission from Bitar et al., 2006.

Due to the interaction of the charged nuclei and the magnetic field, the individual spins will precess (rotate). The rate of precession depends on the strength of the external magnetic field. The nuclear spin vector has the same direction as B_0, but the precession of the spinning nucleus as a whole is at an angle to B_0. MR applications, such as MRS and MRI, are based on the fact that the precessing spins can be temporarily adjusted by a RF pulse, which simultaneously flips the spins toward the x,y plane resulting in a signal that is in phase. This means that the spins are at the identical point of their rotation simultaneously. The exact frequency at which it is possible to acquire this depends on the strength of the B_0 and is called the Larmor frequency. (Pooley 2005)

Larmor equation

$$f_0 = (\gamma \times B_0) / 2\pi$$

states that the nucleus resonance frequency f_0 (Hz) is proportional to the static magnetic field B_0 (T). γ is the gyromagnetic ratio, which is specific for each nucleus. For example, at a magnetic field of 3.0 T, the Larmor frequency of a ^{1}H nucleus is 127.74 MHz.

2.3.2.2 MR scanner

MR systems have a constant high magnetic field (B_0), produced by electric current in loops of superconducting wire. Liquid helium keeps the temperature low enough to enable the superconducting state. Consequently, current can be retained in the coil for years without recharging. Typically, scanners used in clinical imaging have the magnetic field of 1.5 Tesla (T) or 3.0 T (Pooley 2005). The magnitude of this magnetic

field is relatively strong. A 3.0 T field strength amounts to 60,000 times the average of the Earth's magnetic field (Siemens 2009).

MRI uses variable magnetic fields superimposed on B_0, produced by gradient coils, to encode the location of a voxel in three-dimensional space. The gradient coils adjust the magnetic field in a selected area linearly. The localization information for the three dimensions is acquired by 1) the excitation of a certain section, 2) the phase, and 3) the frequency of the MR signal in the imaged area. Typically, the longitudinal z-axis is aligned with the main magnetic field (B_0). The x- and y-axes form a perpendicular transverse plane. (Bitar et al. 2006; Pooley 2005)

By allocating the area imaged to these smaller volumes, or voxels, the signal from the voxels can be measured individually. By repeating the process, information can be gathered to reconstruct a series of MR images. The MR scanner transmits the RF pulse and observes the signal produced by resonating nuclear spins using dedicated receiving coils. (Pooley 2005)

Gradient coils encode the location of a voxel in a three-dimensional space (Bitar et al. 2006; Pooley 2005). The gradients create linear differences in a selected region of the magnetic field strength (Bitar et al. 2006). In typical cylindrical-bore MR scanners the longitudinal z-axis is aligned with the main magnetic field. (Bitar et al. 2006; Pooley 2005)

RF coils both transmit and receive MR signal. Transmitter RF coils cause a change in the direction of the nuclear spins. The resulting signal produced by resonating nuclear spins located in the tissue is detected by the receiver RF coil. The coils can be different in size depending on the target area. (Turner 1993)

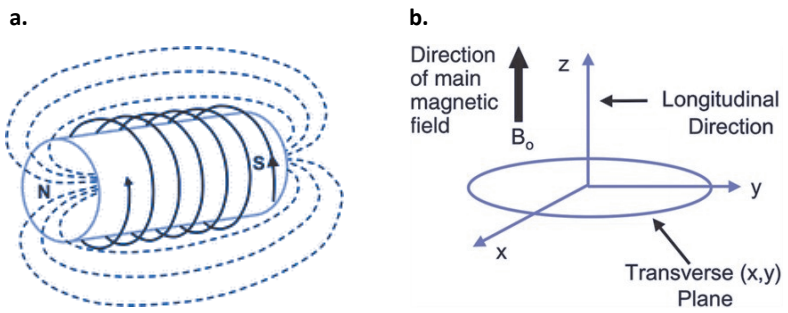

Figure 3. **a)** Main magnetic field (B_0) of MR scanners. N=North, S=South. **b)** Three-dimensional coordinate system for MR scanners. The longitudinal magnetization is typically horizontal and aligned with the patient's longitudinal axis, for example, head to feet. Accordingly, the transverse plane corresponds to the patient's axial direction. Modified and reprinted with permission from Pooley, 2005.

2.3.2.3 T1 recovery

The RF pulse temporarily flips the spins, which realign to the static magnetic field B_0 when the RF pulse is no longer applied. The nuclei release the excess energy to the environment when they realign to their longitudinal direction (Pooley 2005; Bitar et al. 2006). This phenomenon is called spin-lattice relaxation, described by the longitudinal relaxation time (T1). Increasing longitudinal magnetization is a process known as T1 recovery (Bitar et al. 2006). T1 relaxation time (ms) is a constant that is different for water and fat, and characteristic to each tissue.

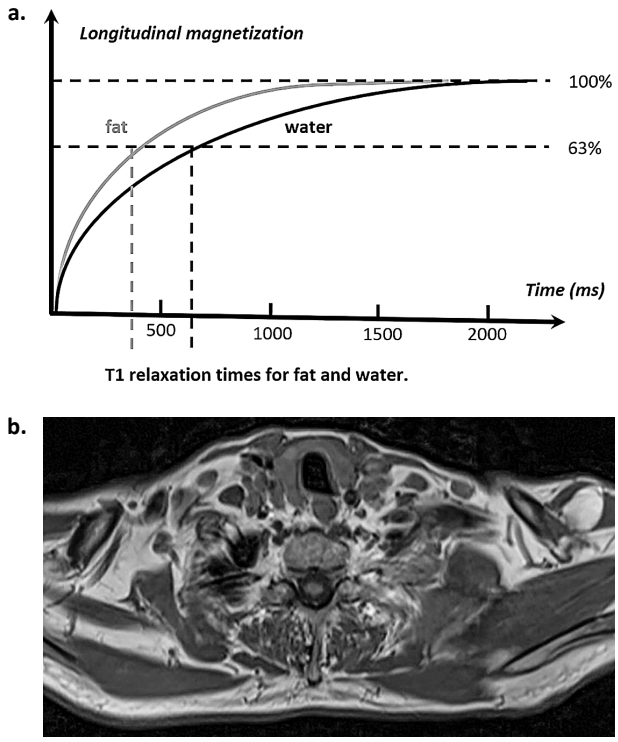

Figure 4. **a)** T1 recovery occurs after the RF pulse has been turned off and the magnetic vector starts to return back toward longitudinal (M_z). The T1 time (ms) is defined as the time it takes for 63% of the longitudinal magnetization to be restored. Water and fat have different T1 relaxation times. **b)** T1-weighted axial MR image of the supraclavicular fat depot.

2.3.2.4 T2 decay

T2 decay is a simultaneous phenomenon with T1 recovery. While flipping the spins toward the x,y plane, the RF pulse also phases the spins temporarily, causing them to be at the identical point of their rotation simultaneously. After the RF pulse is turned off, the spin-spin interactions cause the transverse magnetization to reduce at a certain speed, as the nuclei begin to dephase. This phenomenon is called transverse or spin-spin relaxation, described by the transversal relaxation time (T2).

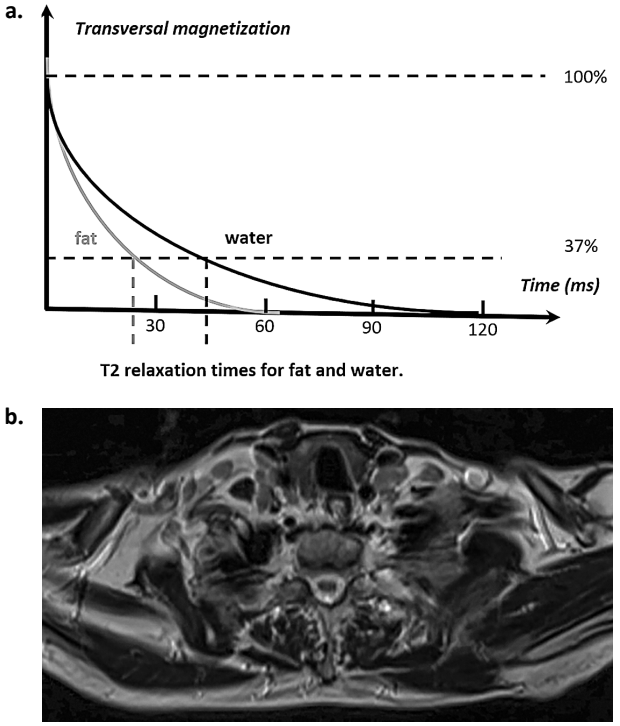

Figure 5. **a)** T2 decay occurs after the RF pulse has been turned off. Transversal magnetization (M_{xy}) starts to diminish as the nuclei lose their coherence phases. T2 time (ms) is defined as the time it takes for 63% of the longitudinal magnetization to be decayed, i.e. 37% of the magnetization is left. Water and fat have different T2 relaxation times. **b)** T2-weighted axial MR image of the supraclavicular fat depot.

2.3.2.5 T2* decay and T2* mapping

T2* mapping measures local susceptibility-induced distortions in the magnetic field caused by the iron content. Gradient echo-based sequences are used, due to their sensitivity to susceptibility artifacts. T2* time is a constant typical for each tissue. (Pooley 2005)

In ideal circumstances, transverse magnetization decay is caused by the natural spin-spin interactions at the molecular level (T2 decay). In reality, transverse magnetization decays much faster than would be predicted by natural atomic and molecular mechanisms, due to the local magnetic field inhomogeneities (Chavhan et al. 2009). In both T2 and T2* relaxation, spin-spin relaxation causes dephasing within the tissue, but magnetic field inhomogeneities arising from the main magnetic field and from differences in magnetic susceptibility, chemical shift effects, and gradients applied for spatial encoding also contribute to T2* decay. Thus, the observed or effective transverse magnetization decay is called T2* decay. T2* is always less than or equal to T2. (Pooley 2005)

Magnetic susceptibility is a quantitative measure of the extent to which a substance tends to interact and distort an applied external magnetic field. Materials that disperse the main field are called diamagnetic. Materials that concentrate the field are called paramagnetic, superparamagnetic, or ferromagnetic, depending on the magnitude of the effect. (Schenck 1996)

Brown adipocytes have more mitochondria than white adipocytes. Also, blood perfusion and oxygen consumption in BAT increase when the tissue is stimulated (Din et al. 2016), and consequently BAT has higher levels of deoxyhemoglobin. Mitochondria and deoxyhemoglobin are both rich in iron, which contributes to the susceptibility effect and thus the lower T2* relaxation time in BAT.

The T2* decay time in each voxel is measured by imaging the volume of interest several times with different echo times (TE). Voxel-based T2* relaxation time maps are calculated by using the linear curve fitting for each subject (Seo et al. 2017).

2.3.2.6 In/opp imaging, Dixon method and SFF maps

In most tissues, MR is based on a technique measuring the signals from the protons located both in water and fat molecules, in which the protons precess at a slightly different frequency. The difference in frequency between the main fat peak (methylene) and the water peak is approximately 220 Hz at 1.5T, and 440 Hz at 3T, respectively. With MR techniques such as in-phase and out-of-phase (in/opp) imaging and the Dixon method, the original signal can be divided into the water and fat components. (Siemens 2009)

The Dixon method is based in a technique called (in/opp) MRI, based on different chemical shift in water and fat (Dixon 1984). It is widely clinically used, especially to suppress the fat signal reliably (Ma 2008). This technique takes advantage of the fact that the ^{1}H nuclei precess at different rates depending on their location in either fat or water molecules, and thus at set times (depending on the strength of B_0) they are either exactly in the same phase or exactly in the opposing phase. Two echoes are acquired when the water and fat signal are in opposed phases, and one when the water and fat signal have the same phase (Eggers et al. 2011). Reconstruction of the data of this individual echo times results in two differently weighed images. From the in/opp image signal intensity (SI) it is easy to calculate the following images (Reeder et al. 2011):

1. in-phase = $| SI_{water} + SI_{fat} |$
2. out-of-phase = $| SI_{water} - SI_{fat} |$
3. fat = (in-phase - out-of-phase) / 2 = $[(SI_{water} + SI_{fat}) - (SI_{water} - SI_{fat})] / 2$

4. water = (in-phase + out-of-phase) / 2 = $[(SI_{water} + SI_{fat}) + (SI_{water} - SI_{fat})] / 2$
5. Signal-fat-fraction (SFF) = fat / (water + fat) = (in-phase - out-of-phase) / 2(in-phase) = $SI_{fat} / (SI_{water} + SI_{fat})$

Thus, the Signal-fat-fraction (SFF) map is an image showing in greyscale the percentage of signal caused by triglycerides in each voxel, the numeric value varying from 1 to 100%. This relative value calculated from the signal of water and fat value does not correspond exactly to the amount of water and triglycerides measured in the tissue due to the presence of other molecules besides water and triglycerides. With these parameters there was moderate T1 and T2 bias as well as T2* decay, which were not corrected, so these SFF measurements give somewhat higher values than true corrected proton density fat fraction imaging (Reeder et al. 2011).

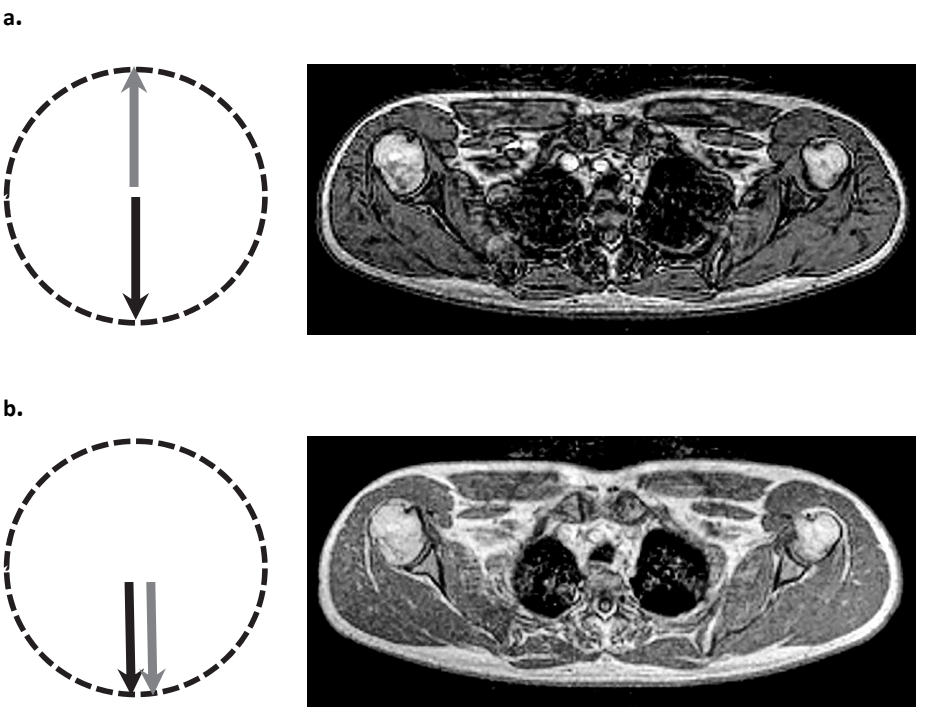

Figure 6. In-phase and out-of-phase MR imaging at 3T. The arrows indicate the direction of the fat and water signal vector at 1,1 ms (a) and 2,2 ms (b), resulting in either **a.** subtraction of signal (out-of-phase) or **b.** addition of signal (in-phase) in the corresponding MR images. Fat only, water only, and SFF images can be calculated from these images.

The method has been widely used to examine human BAT (Chen et al. 2013; Deng et al. 2015; Franz et al. 2015; Hu, Yin, et al. 2013; Lundstrom et al. 2015; Stahl et al. 2016). It has even been used to measure the triglyceride content dynamically, as a response to BAT stimulation. Romu et al. used a rat model to prove that SFF mapping

is a reliable technique for measuring differences in BAT volume and triglyceride percentage during cold exposure (Romu et al. 2015). Lundstrom et al. measured decreased fat fraction due to BAT lipid consumption during a cooling-reheating protocol (Lundstrom et al. 2015).

2.3.2.7 Proton Magnetic Resonance Spectroscopy (^{1}H MRS)

Single-voxel proton magnetic resonance spectroscopy (^{1}H MRS) is a noninvasive and sensitive clinical application for acquiring biochemical information in vivo, by measuring the amount of endogenous metabolites in tissue, for example quantifying tissue triglyceride content. Instead of producing an anatomical image, MR spectroscopy uses the information from the observed signal to provide a frequency spectrum of a single voxel, describing the intensity of the MR signal as a function of precession frequency (Lundbom et al. 2010).

The method has been used to measure water and triglyceride content in adipose tissue, the liver, skeletal muscle, and bone marrow (Schrover et al. 2014; Ojanen et al. 2014; Kato et al. 2014; Borra et al. 2008). BAT contains both water and fat, so it is an ideal target for ^{1}H MRS measurements. The water peak can be identified at 4.7 ppm and the main fat peak of methylene $(CH_2)_n$ at 1.3 ppm. Methylene is an indicator of the chain length of the fatty acid, which varies due to the chain length and interruptions caused by double bonds.

Besides the quantity of triglycerides in the fat tissue, the chemical composition of fat often provides useful information. For this purpose, other smaller magnitude fat peaks are also measured with ^{1}H MRS. The methyl (CH_3) peak at 0.9 ppm can be used as an internal reference for the number of fatty acid molecules, since each triglyceride structure contains nine methyl protons. β-methylene at 1.6 ppm is also characterized by a defined number of protons per triglyceride, while the peak of allylic protons at 2.0 ppm reflects the number of unsaturated vinyl groups. (Bottomley and Griffiths 2016)

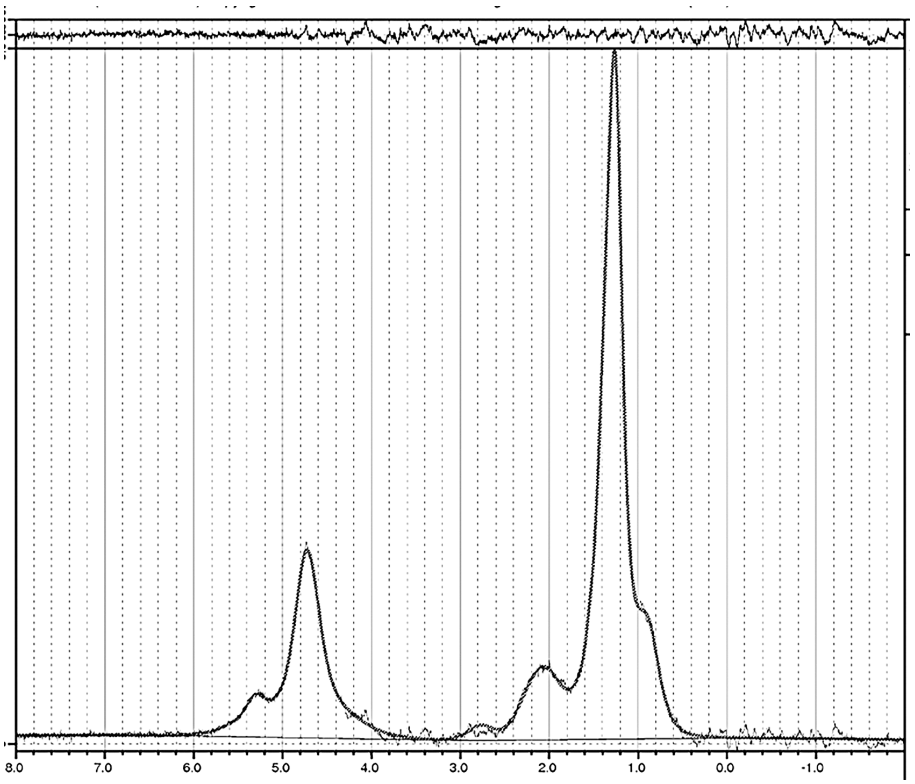

Figure 7. Example of a typical ^{1}H-MRS spectrum of supraclavicular BAT tissue. The analyzed spectrum shows a characteristic peak at 4.7 ppm representing water. The main fat peak of methylene $(CH_2)_n$ at 1.3 ppm is considerably higher, demonstrating the fat component of tissue being larger than the water component. Other smaller magnitude fat peaks are also shown, such as the methyl (CH_3) peak at 0.9 pp and allylic proton peak at 2.0 ppm.

2.3.2.8 Fat and Water Suppression techniques

Fat or water suppression techniques, such as Spectral Presaturation with Inversion Recovery (SPIR), have not been used widely in BAT imaging. They separate the tissue MR signal into its fat and water components by comparing magnitude images acquired with and without chemical fat saturation. A potential problem with these suppression techniques is that the complete and homogeneous suppression of either fat or water signal by the selective excitation pulse is difficult if not impossible to reliably achieve throughout the whole imaged area, due to inhomogeneous main magnetic field (B_0). The method is only valid when assuming perfect suppression. As a sequence, Dixon method is decidedly more robust and easier to use. (Reeder et al. 2011)

At the time of the design of Study I, there was no literature of fat or water suppression techniques in BAT imaging. More recently, there is a single study on humans on water saturation efficiency measurement (Chen et al. 2013).

2.3.2.9 Other MR imaging methods of BAT

Other MR imaging methods that have been used to examine BAT include blood-oxygen-level-dependent (BOLD) functional MRI (fMRI) (van Rooijen et al. 2013; Chen et al. 2013) and diffusion weighted imaging (DWI) (Deng et al. 2015).

2.3.3 Other methods for examining BAT

Experimental methods being used to investigate BAT include computed tomography (CT), infrared termography (IRT), and contrast ultrasonography (US) (Sun et al. 2017). The results are still preliminary.

In computed tomography, the radiodensity of BAT tissue is measured in Hounsfield Units (HU) from noncontrast CT images. The change in HU is assumed to be due to increased perfusion and decreased triglyceride content in BAT following metabolic activation. However, in general clinical and imaging purposes, the tissue contrast and sensitivity for soft tissue imaging are considered better in MR imaging than in CT imaging. (Ahmadi et al.)

In infrared termography, the temperature of the skin is measured at the supraclavicular area. The increase in difference of temperature on the skin directly overlying the supraclavicular area and the skin elsewhere on the chest is considered to reflect the increased metabolic activity in BAT tissue. (Jang et al. 2014)

Contrast ultrasonography involves the application of the ultrasound contrast medium to traditional medical sonography (McCulloch et al. 2000). Ultrasound as an imaging modality relies on the reflection of sound waves from interfaces between different substances and tissues. Commercially available contrast media are gas-filled microbubbles that are administered intravenously to the systemic circulation. Microbubbles have a high degree of echogenicity and are able to produce a sonogram with increased contrast due to the high echogenicity difference. Contrast-enhanced ultrasound can be used, for example, to measure perfusion and blood flow rate in BAT. (Sun et al. 2017)

3 AIMS OF THE STUDY

I To develop MR pulse sequences to examine adipose tissue, notably to determine the existence of BAT, to quantify the amount of BAT, and to estimate the metabolic activity of BAT. (Studies I - III)

II To apply ^{1}H MRS to investigate the triglyceride content of BAT and WAT, and the association with metabolic markers, on both lean and obese patients. (Study II)

III To measure BAT, WAT and muscle SFF and T2* values during cold exposure and at ambient conditions and examine whether cold exposure affects these MRI measurements. (Study III)

IV To compare MRI and PET in imaging BAT. (Studies I – III)

4 SUBJECTS AND STUDY DESIGN

The research consisted of three studies. Study I included an animal study. All three studies (studies I-III) included examinations of healthy human volunteers. The overall study outline is presented in Table 1.

Table 1. Outlines of studies I-III and general characteristics of the study subjects.

Study	Model	Study group	N (M/F)	Age (yrs)	BMI (kg/m^2)	Biopsy	Cold exposure	Objective
I	rat	normal weight	11 (11/0)	-	-	All (11/11)	Rats: PET and MRI in ambient conditions. Humans: PET in cold conditions, MRI in ambient conditions.	To differentiate BAT from WAT in rats using DUAL-SPIR MRI
	human	normal weight	3 (1/2)	35.6 ±12.3	23.7 ±0.3	None (0/3)		
II	human	normal weight	12 (0/12)	36.9 ±10.1	21.9 ±1.9	Some (8/12)	PET in cold and ambient conditions, ^{1}H MRS only in ambient conditions	To investigate the triglyceride content of BAT and WAT and their association with metabolic markers
		obese	13 (1/12)	40.4 ±9.5	32.2 ±5.0	Some (1/12)		
III	human	normal weight	9 (5/4)	30.9 ±8.9	22.9 ±1.4	None (0/9)	MRI in cold and ambient conditions, PET only in ambient conditions	To measure BAT, WAT and muscle MRI properties and examine whether cold exposure affects these
		Overweight and obese	4 (2/2)	36.0 ±11.7	26.5 ±3.7	None (0/4)		

4.1 STUDY SUBJECTS

4.1.1 Rat model (Study I)

Study I was performed on a rat model. The animal study protocol was reviewed by Ethics Committee for Animal Experimentation at the University of Turku, Finland and was approved by the State Provincial Office of Western Finland (STH39A//ESLH-2006-11128/Ym-23).

4.1.2 Human subjects (Studies I-III)

For studies I, II and III, a total of 41 volunteers were recruited (3, 25 and 13, respectively): 24 of the subjects were of normal weight (BMI 20.3-24.9 kg/m2), three were overweight (BMI 25.0-31.5 kg/m2) and 14 were obese (BMI 31.5 kg/m2). For the definition of obesity, the WHO criteria were used. Both genders were studied (9 M/32 F).

Subjects were recruited through advertisements in a local newspaper and university web page. Volunteers were first interviewed and screened by a licensed physician to exclude subjects with diabetes or other diseases. Subjects with normal glucose tolerance and normal cardiovascular status (assessed on the basis of electrocardiograms and measured blood pressure) were included.

In study II, BAT and WAT biopsies were performed in those 9 subjects (out of total 25) who provided separate written informed consent for the procedure. Eight of those subjects were lean, and one was obese.

All subjects included in studies I-III gave written informed consent before their participation. The studies were conducted according to the guidelines of the Declaration of Helsinki and furthermore the study protocol was approved by the Ethics Committee of the Hospital District of Southwest Finland.

4.2 STUDY DESIGN

4.2.1 Animal model (Study I)

Eleven male Sprague-Dawley rats, weighing 325-400 g, bred at the animal facility of the University of Turku, were housed under standard room temperature conditions (20 ± 1 ˚C, humidity 55 ± 5%, lights on from 6:00 a.m. to 6:00 p.m.) with free access to standard food and tap water. Because the local Ethics Committee did not grant permission for cold exposure of the rats, they were not exposed to cold. On a given study day, an ^{18}FDG-PET/CT scan was performed first, followed by an MR study.

The animals were anesthetized via isoflurane inhalation during the ^{18}FDG-PET/CT scan and then euthanized by carbon dioxide ($CO_{2)}$ gas prior to the MR studies. A dual-echo (in/opp) sequence was used, both with and without spectral presaturation inversion recovery (SPIR) fat suppression (DUAL-SPIR) to visualize BAT. After the MR scan, the BAT tissue of the rats was located visually through careful dissection, and it was then removed and weighed. The removed BAT tissue was also immunohistochemically stained and analyzed. Measurements of BAT volumes obtained with ^{18}FDG-PET/CT and DUAL-SPIR MR were quantitatively compared to the histological findings. All of the rats were euthanized approximately 5 hours prior to the BAT dissection and histological analysis.

4.2.2 Human model (Study I)

Three healthy human subjects, one male and two females of normal weight, were exposed to cold conditions prior to ^{18}FDG-PET/CT examination. MR examination

was performed at a later time under normal warm conditions. The MR parameters were almost identical to those applied on rats, excluding the FOV and slice thickness, which were considerably larger, accommodating the size of imaged area.

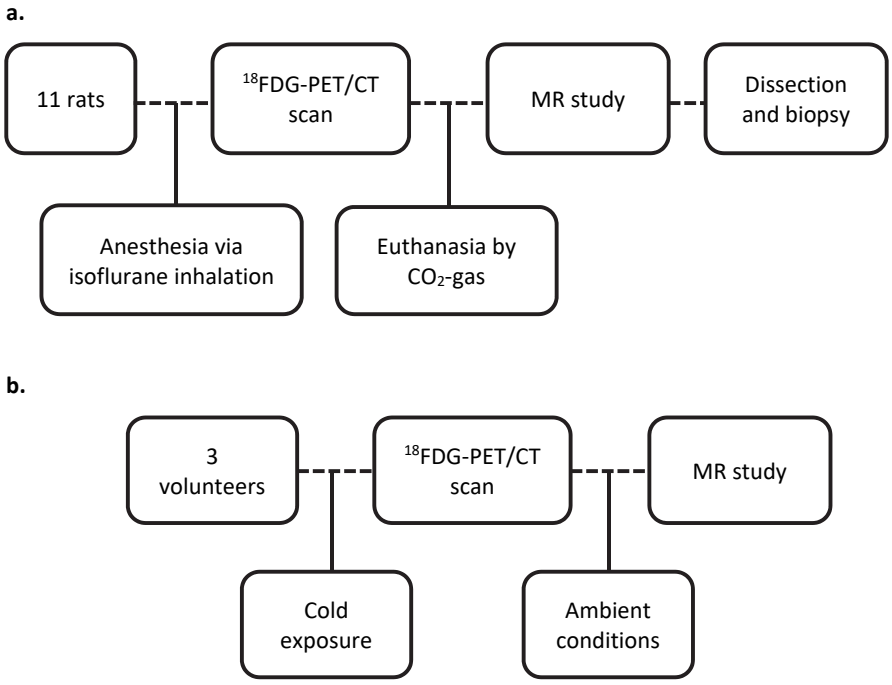

Figure 8. Study design (I) outlined on rat model (a) and on humans (b). The volume of the BAT depot was measured on a ^{18}FDG-PET/CT scan and a DUAL-SPIR MRI.

4.2.3 Study II

Study II consisted of 25 volunteers (1 M/24 F): 13 of the subjects were obese (1 M/12 F) and 12 normal weight (0 M/12 F). ^{18}FDG-PET and ^{15}O-H_2O PET perfusion studies were performed on all 25 subjects, using either a hybrid PET/CT scanner (n=11) or a stand-alone PET scanner (n=14). Each subject was scanned twice on separate days, both after cold exposure and during ambient conditions.

^{1}H MRS and MRI were performed on 22 of the 25 subjects (1 M/21 F). The examination was conducted in ambient room temperature conditions without specific preparations. An MRI scan was obtained to provide anatomical reference in the neck and body area and also to measure the intra-abdominal and subcutaneous fat volume. The scan that was obtained in warm conditions was performed on a separate day, with the same scanning protocol but without the cold exposure. Both scans were conducted after the subject had fasted overnight.

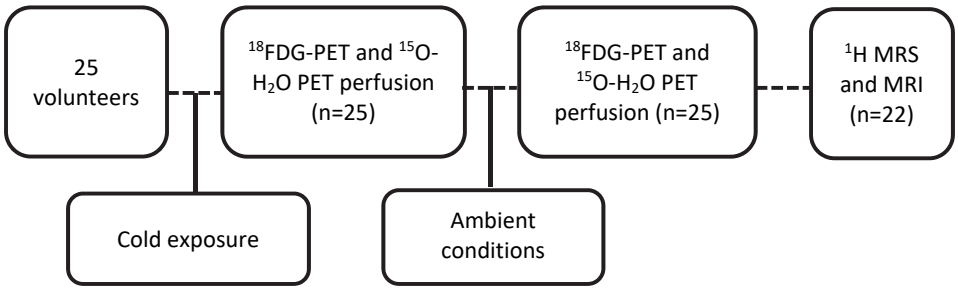

Figure 9. Study design (II) outlined. The triglyceride content of the supraclavicular BAT depot was measured with ^{1}H MRS and correlated with PET activation measured with ^{18}FDG-PET/CT ^{15}O-H_2O PET perfusion scans.

4.2.4 Study III

Another group of volunteers (n=13, 7 M/6 F) was recruited to further study MR imaging techniques at 3T PET/MRI: 4 of the subjects were obese (2 M/2 F) and 9 normal weight (5 M/4 F). MRI scans were obtained twice, during cold exposure and in warm conditions. All scans were obtained in the morning, between September and April. The mean time between the scans of each individual was 24 ± 27 days.

The first imaging session started with cold exposure, followed by a dynamic ^{18}FDG-PET examination and an MR scan. The second session consisted only of an MR scan. Thus, the triglyceride content of BAT and WAT tissue on the neck and supraclavicular area as well as that of supraspinatus muscle were measured using SFF and T2* time mapping, both during cold exposure and in ambient conditions. ^{18}FDG-PET was performed only during cold exposure, to avoid the radiation burden associated with recurring PET examinations.

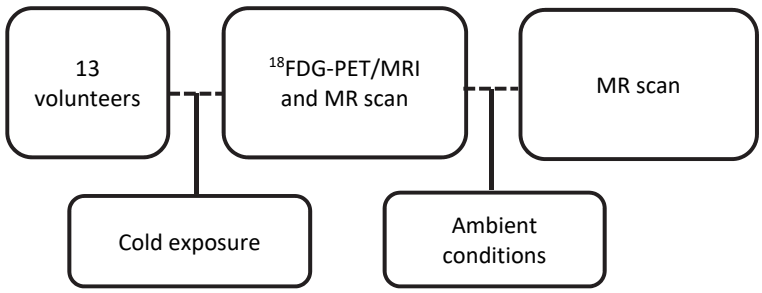

Figure 10. Study design (III) outlined. The outline of the supraclavicular BAT depot as well as VOIs on WAT and supraspinatus muscle were drawn on SFF map images, and these exactly same coregistered VOIs were used to measure SFF, T2* time and ^{18}FDG uptake in corresponding images.

5 MATERIALS AND METHODS

5.1 ANTHROPOMETRIC MEASUREMENTS (Studies I-III)

Studies II and III were conducted on humans, as well as a study of 3 healthy volunteers which was conducted as a part of study I. Basic anthropometric measurements were performed on all participants. Waist circumference was measured at the navel level and hip circumference at the major trochanter level. Weight was determined using weighing scales (Seca, Hamburg, Germany) and height with a measurement tape. Body mass index was calculated as the weight in kilos divided by the height in meters squared. Blood pressure was measured three times using a sphygmomanometer (Omron, Kyoto, Japan) in the prone position, and the mean values were used.

5.2 LABORATORY STUDIES (Study II)

In study II, laboratory tests were performed on all participants. Serum total cholesterol and high density lipoprotein (HDL) cholesterol were determined from serum samples after overnight fasting. The low density lipoprotein (LDL) cholesterol concentration was calculated using the Friedewald formula when the serum triglycerides were <4.0 mmol/l. Plasma glucose measurement and a two-hour oral glucose tolerance test (OGTT) were performed after overnight fasting. The study subjects drank approximately 330 ml of liquid containing 75 g glucose. Venous blood samples for the determination of fasting glucose and insulin and glucose at 120 min were obtained.

5.3 HYPERINSULINEMIC CLAMP (Study II)

Insulin sensitivity (M-value) measurements were based on a 2-hour euglycemic hyperinsulinemic clamp study. The serum insulin was increased for approximately 160 min using a primed-continuous 1 mU / kg / min infusion of insulin (DeFronzo, Tobin, and Andres 1979). Normoglycemia was maintained using a variable infusion rate of 20% glucose, based on venous plasma glucose measurements.

5.4 CALCULATING RISK SCORES (Study II)

A subject's 8-year risk for diabetes was estimated based on the Framingham diabetes risk score (Wilson et al. 2007) and the 10-year risk of cardiovascular disease (CVD) with the Framingham CVD risk score (D'Agostino et al. 2008).

5.5 COLD EXPOSURE (Studies I-III)

The subjects underwent cold exposure to metabolically activate BAT.

In study I (human volunteers) and II, the cooling was achieved using ice water. Before the cold-exposure scan, the subject, while wearing light clothing, spent 2 hours in a room that had an ambient temperature of 17 to 19°C. While the PET/CT study was being performed, one of the subject's feet was placed intermittently in ice water (5 to 9°C; 5 minutes in the water alternating with 5 minutes out).

In study III, the cold exposure was obtained by using special cooling blankets. Before being positioned in the scanner for the cold-exposure scan, the subject, while wearing light clothing, spent 120 minutes lying on a bed with a water circulated cooling blanket (Blanketrol III, Cincinnati Sub-Zero, Cincinnati, OH, USA) beneath their trunk and legs and a similar blanket on top of them. The temperature of the water inside the blanket was first set to +5°C and then adjusted accordingly in order to achieve non-shivering thermogenesis by raising the temperature of the blankets if the subject was shivering. During the 3T PET-MR scan, cold exposure was maintained by placing cold packs around the lower extremities of the subject.

5.6 BIOPSIES AND HISTOLOGY

5.6.1 Rat model (Study I)

After imaging, the rats were euthanized and all visible BAT was carefully dissected in all eleven rats. Immediately upon dissection, the brown adipose tissue was immersed and fixed in 10% buffered formalin (pH 7.4) and subsequently embedded in paraffin. Five-micrometer sections were cut and stained with hematoxylin and eosin. The histological criteria for the tissue to be labeled as brown fat were the following: dense capillary vasculature; typical multiple small vesicles in the cytoplasm; and strong eosinophilic cytoplasmic staining (rather than a single fat droplet observed in the white adipose tissue cells). Using both morphological and immunohistochemical methods, more than 90% of the dissected tissue was

confirmed to be BAT. The remaining tissue was composed of small amounts of fibro-fatty tissue, vessels, and muscle.

5.6.2 Human studies (Study II)

Biopsies were performed in those 9 subjects (out of total 25) who provided separate written informed consent for the procedure. Eight of those subjects were lean, and only 1 was obese. The ^{18}FDG-PET images were used as references for the location of BAT for the biopsy and ^{1}H MRS planning. The biopsy was performed under local anesthesia (lidocaine supplemented with epinephrine). A plastic surgeon biopsied the supraclavicular fat deposit from areas that corresponded to the cold-induced areas of uptake in high-resolution ^{18}FDG-PET. Immediately following the removal, the tissue sample was either frozen or prepared for further histological studies and examined as described in the supplementary appendix.

5.7 MAGNETIC RESONANCE IMAGING METHODS

Study I and II were conducted in ambient room temperature conditions without specific preparations with a Philips Gyroscan Intera CV Nova Dual 1.5T MRI scanner (Philips Medical Systems, Best, the Netherlands). The system was equipped with an internal body coil. A circular C3 surface coil (for study I rat model) and a flexible E1 surface coil (for study II and study I human volunteers) was used for the MRI studies.

Study III was conducted using a Philips Ingenuity 3T PET/MR scanner (Philips Healthcare, Cleveland). The MR examination was performed using a two-channel whole body RF coil for excitation, while signal was measured using a 32-channel cardiac coil. Both MRI and PET measurements were performed during the same examination. MR measurements were performed in the supraclavicular and neck area.

Both MRI scanners were located at the Turku PET Centre.

5.7.1 Dixon imaging as anatomical reference (Studies I, II)

For study II and study I human volunteers, a standard dual-gradient echo in/opp sequence MRI was used to provide anatomical references in the neck and body area and also to measure the intra-abdominal and subcutaneous fat volume for the body area. A dual-gradient echo in/opp sequence was used with a repetition time (TR) of 120 ms, echo times (TE) of 1.15 ms and 4.60 ms and flip angle (FA) of 80°. The acquisition matrix was 256 x 128 with foldover suppression, the field of view (FOV) was 530 mm, and the slice thickness was 4 mm. SFF maps were not generated.

In the rat model, a standard dual-gradient echo in/opp sequence was used as an anatomical reference, with a repetition time (TR) of 10.1 ms, echo times (TE) of 2.30 ms and 4.60 ms, flip angle (FA) of 80°, and two averages. The acquisition matrix was 240 x 240 with foldover suppression, the field of view (FOV) was 140 mm, and the slice thickness was 0.5 mm with a 0.1 mm gap between adjacent slices. In total, 70 sagittal and 70 axial slices of the interscapular area were obtained.

5.7.1.1 Measuring intra-abdominal and subcutaneous fat volume (Study II)

The MRI slices on the anatomical reference Dixon in-phase sequence between the apex of the heart and the femoral heads were used for measuring the abdominal and subcutaneous fat volume. ROIs were drawn on continuous slices on the anatomical intra-abdominal and subcutaneous fat tissue. The fat volumes were measured using Sliceomatic 5.0 software (TomoVision, Quebec, Canada).

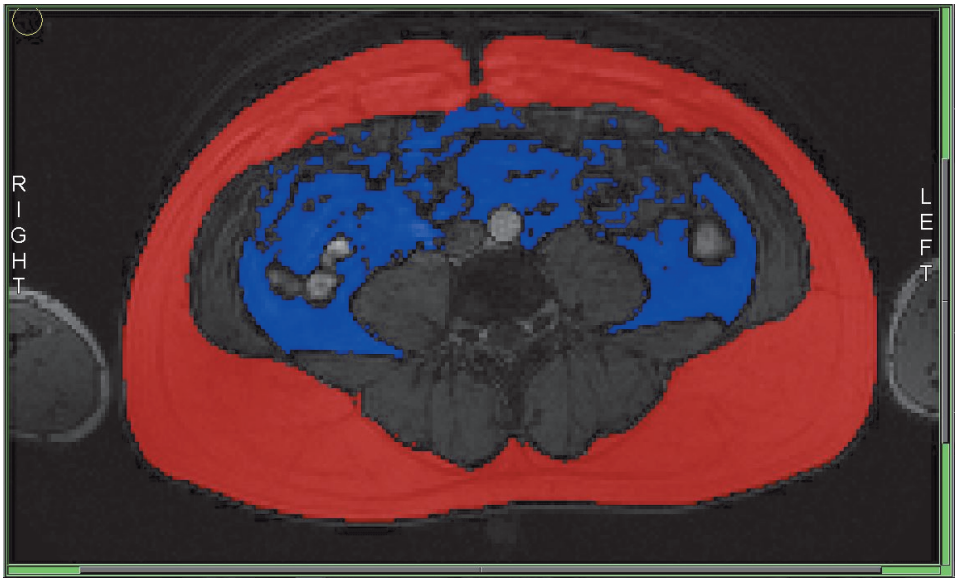

Figure 11. Measuring intra-abdominal and subcutaneous fat volume in the Dixon in-phase MR images using Sliceomatic 5.0 software.

5.7.2 DUAL-SPIR (Study I)

5.7.2.1 DUAL-SPIR imaging in rat model (Study I)

The standard Dixon imaging sequence described above was combined with a spectral presaturation inversion recovery (SPIR) pulse, which preceded the dual-echo acquisition, a method termed DUAL-SPIR. The inversion pulse (Tanaka et al. 2007) was adjusted such that the zero crossing of the T1 relaxation of the lipid signal

occurred at the center of the excitation pulse. During the multi-slice scans, a fat suppression pulse was applied before every slice. These DUAL-SPIR images were obtained from six rats, and all of the other parameters, except for the addition of the SPIR pulse, were identical to the conventional in/opp imaging series described above.

5.7.2.2 DUAL-SPIR imaging in human subjects (Study I)

MR examination was performed on three healthy human volunteers under normal ambient conditions. The imaging parameters were as similar as possible to those used in the animal studies: field of view (FOV), 530 mm; acquisition matrix, 256 x 179; slice thickness, 4 mm with a 0.4 mm gap between adjacent slices; repetition time (TR), 120 ms; echo time (TE), 2.30 ms and 4.60 ms; and flip angle (FA), 80° and one average. A number of slices covering the entire cervical-supraclavicular region were selected and were obtained both with and without the presence of a spectral presaturation inversion recovery (SPIR) pulse.

5.7.2.3 Image data postprocessing (Study I)

The MRI images were postprocessed by subtracting the out-of-phase images from the in-phase images within both the series of conventional in/opp data and the DUAL-SPIR data, essentially generating a fat-only image Dixon image (as described in section 2.3.2.4).

Postprocessing was performed on a Siemens Leonardo workstation (syngo MMWP VE27A, Siemens AG, Berlin and Munchen). Brown adipose tissue, as defined by the remaining bright interscapular signal intensity in each subtraction series, was outlined in each consecutive slice using a freehand ROI tool. The outlined tissue volume was calculated offline by multiplying the outlined areas by the slice thickness, also taking into account the interslice gap.

The MR images, the originals and the images obtained from the subtraction series, were also fused with the PET images to facilitate a more direct comparison between the two modalities. This fusion was accomplished using the Mirada 7D software package on a PET/CT workstation (Mirada Solutions Ltd., Oxford, England). Through co-registration of the anatomical MR and CT data and application of the same transfer matrix to the PET data and the acquired subtraction MR data, highly accurate fusion of the MR and PET data was obtained.

5.7.3 ^{1}H MRS imaging (Study II)

^{1}H-MRS examination was conducted in ambient room temperature conditions without specific preparations using a Philips Gyroscan Intera CV Nova Dual 1.5T MRI

scanner (Philips Medical Systems, Best, the Netherlands) with the SENSE body coil, with normal preprosessing steps such as shimming, but no ECG or respiration gating. A pointed-resolved spectroscopy (PRESS) ^{1}H-MRS sequence was used with a repetition time (TR) of 3000 ms, echo time (TE) of 25 ms and number of signal averages (NSA) of 4. The sample frequency of 1000 was used with 2048 samples. T2 correction was not applied.

The size of the voxel was optimized and adjusted for each subject in order to avoid the surrounding muscles, and 4 saturation bands were used. Typical voxel size was 10 mm x 10 mm x 12 mm. ^{1}H-MRS measurements were performed in both the supraclavicular fat depot and in the subcutaneous WAT of the neck area (Fig. 12). Scout views were acquired with good resolution in 3 planes by an experienced technician and physicist. After that, an expert physician specialized in BAT located the most probable anatomical location of BAT, based on previous PET studies and general knowledge of BAT anatomy. Great care was taken to place the voxel inside the fat deposit and to avoid all contamination by muscle tissue or vessels.

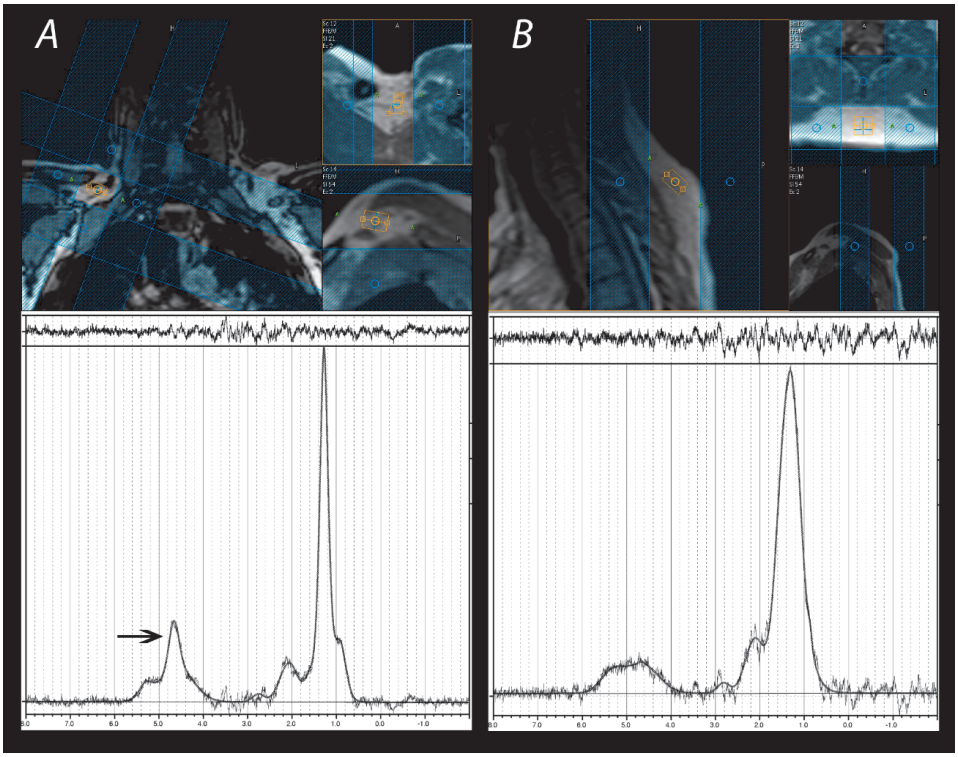

Figure 12. ^{1}H-MRS of supraclavicular BAT and subcutaneous WAT. Positioning of the ^{1}H-MRS voxel. The analyzed spectrum of the voxel in the supraclavicular fat depot (a) shows a characteristic peak at 4.7 ppm that represents water (black arrow). The analyzed spectrum of the MRS voxel in the subcutaneous white adipose tissue (b) shows a smaller water peak. Reprinted from study II.

5.7.3.1 ^{1}H MRS Data analysis (Study II)

^{1}H MRS data were analyzed using the LCModel version 6.2-1L software (Provencher 2001). Lipid signals at approximately 0.9 ppm, 1.3 ppm, 1.6 ppm and 2.0 ppm were used. Readings were independent, and readers were blinded to other information.

5.7.4 SFF mapping (Study III)

A modified 2-point Dixon sequence (mDixon) was used to provide anatomical reference in the neck and body area and to calculate SFF maps. The mDixon sequence was a FFE 3D based sequence with TE1=1.07 ms, TE2=1.9 ms and TR=3.1 ms. Voxel size was 1.75 mm x 2 mm x 1.5 mm and 133 slices were collected with an acquisition time of 16 seconds. Scans were performed using axial, coronal and sagittal slice orientations. No breath-hold was used.

5.7.5 T2* mapping (Study III)

Fat and water suppressed multi-echo flyback FFE3D scans were performed to obtain T2* maps separately for water and fat. SPIR was used to suppress signal from either fat or water to obtain signal decay free of fat-water resonance frequency difference modulation. The TR was 70 ms and the first TE 1.15 ms. Ten echoes with an echo spacing of 1.1 ms were collected. The flip angle was 20 degrees and two averages were collected with voxel size 2 mm x 2 mm x 3 mm. The number of slices was 10 and SENSE factor 2 in the anteroposterior direction. The total scan duration was 2 minutes 56 seconds. No breath-hold was used.

5.7.6 Analyzing SFF, T2* and ^{18}FDG data (Study III)

T2* relaxation maps were calculated using OsiriX v.6.0.2 software (Pixmeo, Geneva, Switzerland). The SFF was calculated from the ratio of the fat signal to the summed water and fat signal and analyzed using commercial Philips software on the MR scanner console. The image series were visually examined by an experienced radiologist to ensure the quality of the data.

Volumes of interest (VOIs) were drawn on semiautomatically including the whole anatomical supraclavicular fat depot using the Carimas 2.9 software package (Turku PET centre, Turku, Finland). The volume of the VOI depended on the size of the subject and the relative size of the supraclavicular fat depot (mean 29.2 ± 9.2 cm^2 after cold exposure, 29.2 ± 10.6 cm^2 at ambient conditions). A rough 3D VOI was drawn on SFF images using the Carimas sphere tool which was subsequently edited with the vertex function, taking great care to avoid the lungs, subcutaneous fat, and bone marrow. Then, the VOI was automatically cropped using the Carimas histogram

tool, with a threshold of 50-100% SFF. The resulting 3D VOI was reduced twice in size using the automatic shrink option, to avoid possible contamination of nearby tissues resulting from chemical shift artifacts or small motion artifacts. The 3D VOIs on subcutaneous WAT and infraspinatus muscle were drawn as ellipsoids using the Carimas sphere tool, assuring an appropriate margin in relation to other tissues.

The SFF data, ^{18}FDG uptake and T2* maps were coregistered and analyzed using the Carimas 2.9 software package using the VOIs described above.

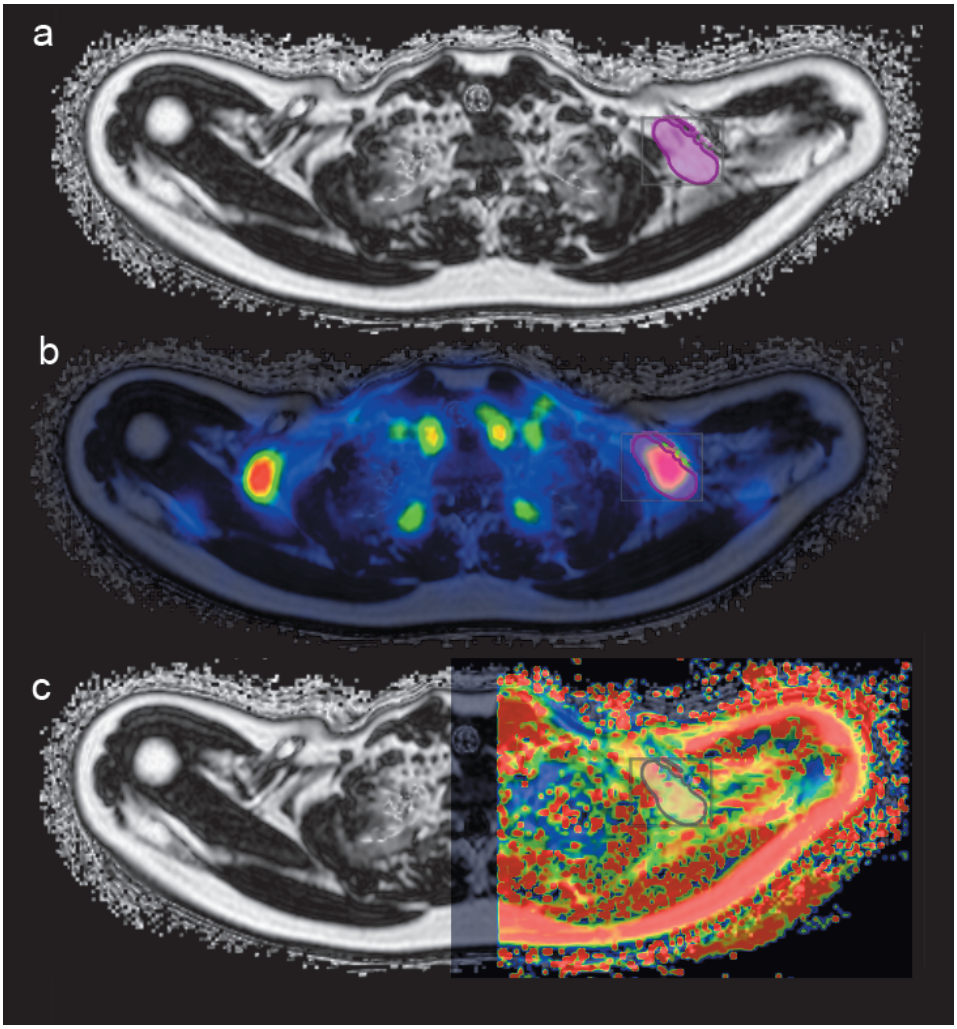

Figure 13. MR and ^{18}FDG-PET imaging (study III). The VOI was drawn semiautomatically on the left supraclavicular fat depot. All the MRI measurements and the glucose uptake measured on ^{18}FDG-PET were calculated using the same VOI. The SFF map **(a)** was calculated from Dixon images. The ^{18}FDG-PET glucose uptake image **(b)** and fat T2* relaxation time map of the left side **(c)** are fused with the SFF map for anatomical reference. Reprinted from study III.

5.8 POSITRON EMISSION TOMOGRAPHY METHODS

All the PET examinations were conducted at the Turku PET Centre. The subjects were advised to fast overnight and avoid exercise for 24 hours and ingesting alcohol or high-fat meals for 72 hours prior to the examination. Room temperature was maintained at approximately 22 °C.

5.8.1 Production of ^{18}FDG (Studies I-III)

^{18}FDG was synthesized in accordance with the standard manufacturing procedures of the Turku PET Centre. A batch of ^{18}FDG was only released for use if the standard operating procedure had been followed. The radiochemical purity exceeded 98%.

5.8.2 Production of ^{15}O H_2O (Study II)

A low-energy deuteron accelerator Cyclone 3 (Ion Beam Application Inc., Louvain-la-Neuve, Belgium) was used for the production of ^{15}O, with a half-life of 123 s. Using a dialysis technique ^{15}O-water (^{15}O H_2O) was produced in a continuously working water module (Sipilä et al. 2001). Sterility and pyrogenity tests were performed to verify the purity of the product. An approximate 97% radiochemical purity of the ^{15}O was obtained.

5.8.3 ^{18}FDG-PET imaging in rat model (Study I)

^{18}FDG-PET/CT scans were performed on eight rats using a hybrid PET/CT animal scanner, Siemens Inveon PET/CT (Siemens Medical Solutions, Knoxville, USA). ^{18}FDG (16.45±0.64 MBq) was injected via a cannula inserted in the tail vein. The rats were anesthetized with isoflurane 60 min prior to a 20-min static PET scan that was preceded by a low-resolution CT scan used for attenuation correction and anatomical reference. The body temperature was not actively influenced or regulated during either the 60-min biodistribution period of ^{18}FDG or the PET/CT scan.

5.8.3.1 Data analysis in rat model (Study I)

The images were reconstructed using an OSEM2D algorithm, and region of interest (ROI) was drawn on the expected BAT tissue and WAT tissue using the areas with high ^{18}FDG uptake and/or the CT anatomical reference scan. The ^{18}FDG uptake of the tissues was quantitatively evaluated by comparing the uptake of the interscapular BAT deposits with subcutaneous white adipose tissue. The volume of the metabolically activated BAT in the ^{18}FDG-PET images was measured using the Mirada

7D software package on the PET/CT workstation (Mirada Solutions Ltd., Oxford, England). The PET scans were analyzed independently, and the reader was blinded to all other information.

5.8.4 ^{18}FDG (Studies I-III) and ^{15}O H_2O perfusion PET (Study II) imaging in humans

^{18}FDG-PET and ^{15}O-H_2O PET perfusion studies were performed in all subjects, using either a hybrid PET/CT scanner or a stand-alone PET scanner. Combined PET/CT studies were performed in 11 of the subjects of study II and all 3 human subjects of study I, using a hybrid PET/CT scanner (Discovery VCT scanner, General Electric Medical Systems, Milwaukee, WI, USA). In 14 of the subjects of study II, PET scans were performed using a stand-alone PET scanner (ECAT EXACT HR+, CTI/Siemens, Knoxville, TN, USA). Both PET tracers were administered via an intravenous catheter into the antecubital vein.

In study II, ^{15}O-H_2O BAT perfusion was performed first. 800 MBq of ^{15}O-H_2O was injected intravenously, and a dynamic scan with variable frame lengths (6 min; 6 x 5 s, 6 x 15 s, 8 x 30 s) was performed. Studies I and III did not include perfusion imaging.

^{18}FDG-PET examination was obtained for all studies in all subjects. A dynamic scan (40 min; 4 x 30 s, 1 x 60 s, 1 x 120 s, 3 x 300 s, 2 x 600 s) of the neck and upper thoracic region was performed simultaneously with a bolus injection of 185 MBq ^{18}FDG. Plasma radioactivity samples were collected during each time frame.

5.8.4.1 ^{18}FDG data analysis

After acquisition of the PET data, the resulting dynamic data were reconstructed. During this process the numerical PET data (i.e. number of counts per detection channel) were converted into PET images. All emission scans were reconstructed with iterative ML-OSEM reconstruction, resulting in a transaxial spatial resolution of about 5 mm in the field of view. The matrix included 128 x 128 pixels. The data from the transmission scans were used to correct the corresponding emission scans for photon attenuation. Furthermore, the PET data were corrected for decay, scattered radiation, and random coincidences.

Summation images of the dynamic PET images were made to obtain a better statistical reference for the co-registration with MRI images. Cold-induced ^{18}FDG uptake in the supraclavicular fat depot was assumed to reflect BAT.

In study II and study I on human subjects, regions of interest (ROIs) were drawn on ^{18}FDG-PET data in the activated area and adjacent planes and also in subcutaneous WAT in the neck area using the Vinci 2.54.0 software package (Max

Planck Institute for Neurological Research, Cologne, Germany). The glucose uptake and volume of activation were calculated using these ROIs.

The ROIs were manually outlined in the fusion image, composed of the summed dynamic ^{18}FDG-PET image and the CT image. The glucose uptake rate value was based on ROIs drawn on 2–3 adjacent transaxial planes on both lateral aspects for defined structures of supraclavicular BAT, and subcutaneous neck WAT was outlined in the midline. Subsequently, regional time activity curves (TACs) were generated.

In study III, SFF data, ^{18}FDG uptake and T2* maps were coregistered and analyzed together with the Carimas 2.9 software package (Turku PET center, Turku, Finland). The process is described above in section 6.8.6.

5.8.4.2 ^{15}O H_2O data analysis

The method of measuring tissue perfusion with ^{15}O H_2O is based on the principle of the exchange of inert gas between blood and tissues (Kety and Schmidt 1945). A two-compartment model including fractional arterial blood volume (de Langen et al. 2008) was linearized and fitted with the subject's whole-blood input function to PET data voxel-by-voxel using the Lawson-Hanson nonnegative least-squares technique to produce parametric perfusion images. The kinetic modeling allows exact quantification even in the presence of flow heterogeneity and the nonuniform partition coefficient of water. ROIs of regional glucose uptake analysis were employed when determining perfusion.

5.9 STATISTICAL ANALYSIS

All tests were performed with SAS, studies I and II with SAS version 9.2 and study III with SAS for Windows version 9.4 (SAS Institute Inc., Cary, NC). P values <0.05 were considered statistically significant.

5.9.1 Study I

In study I, all statistical analyses were performed by an experienced biostatistician. Comparisons between the measurement techniques were performed using paired t-tests. The relationship between the BAT mass obtained through autopsy and imaging methods was calculated using Pearson’s correlation. Agreement between the BAT mass acquired by different imaging techniques and the mass acquired by histology was assessed using Bland-Altman plots.

5.9.2 Study II

In study II, the mean values of continuous normally distributed variables were compared using standard t-tests. Median division was performed based on supraclavicular fat deposit triglyceride content (median level=78.1%) to divide subjects into low- and high-triglyceride content groups. The M-values were log-10-transformed prior to general linear model analysis, and correlation analyses were performed with Spearman's correlation due to the skewed distributions. The correlations were performed with the supraclavicular fat deposit triglyceride content assumed to be a continuous variable. To examine independent associations between supraclavicular fat deposit triglyceride content and obesity-related metabolic markers, general linear models were used, adjusted for age and waist circumference, with the supraclavicular fat deposit triglyceride content as the explanatory variable and the metabolic marker (HDL-cholesterol or log-transformed M-value) as the response variable. Multivariable linear regression models were performed with the M-value as the response variable and the BAT triglyceride content as the explanatory variable. The models were adjusted with age and an obesity marker (BMI, waist circumference or whole-body fat percentage).

5.9.3 Study III

In study III, correlations were performed using Pearson's correlation with the T2* values, SFF values and ^{18}FDG uptake assumed to be continuous variables. A mixed model repeated measures analysis was performed to analyze the possible differences between the examinations acquired during cold exposure and in ambient conditions and to compare the different VOIs (BAT, WAT, muscle).

6 RESULTS

6.1 IDENTIFYING BAT IN EXPERIMENTAL ANIMAL MODEL (STUDY I)

Visually, the BAT was best identified in DUAL-SPIR MRI subtraction ('fat-only') images, compared to nonsubtracted images or conventional in/opp imaging. In both MRI and ^{18}FDG-PET/CT, the assumed BAT was located in the dorsal interscapular fat depot. The volume of activated BAT in ^{18}FDG-PET/CT examination was significantly smaller than the anatomical BAT volume in the MR images (0.05 cm^3 vs 0.19 cm^3, p=0.0016). Three of the eleven rats showed no metabolic activation of BAT in ^{18}FDG-PET, but even in those specimens the anatomical BAT could be measured in DUAL-SPIR MRI.

The amount of BAT measured from the DUAL-SPIR subtraction images showed the best correlation and best agreement with the dissected BAT mass, according to the Bland-Altman analysis, (P=0.017, R=0.89).

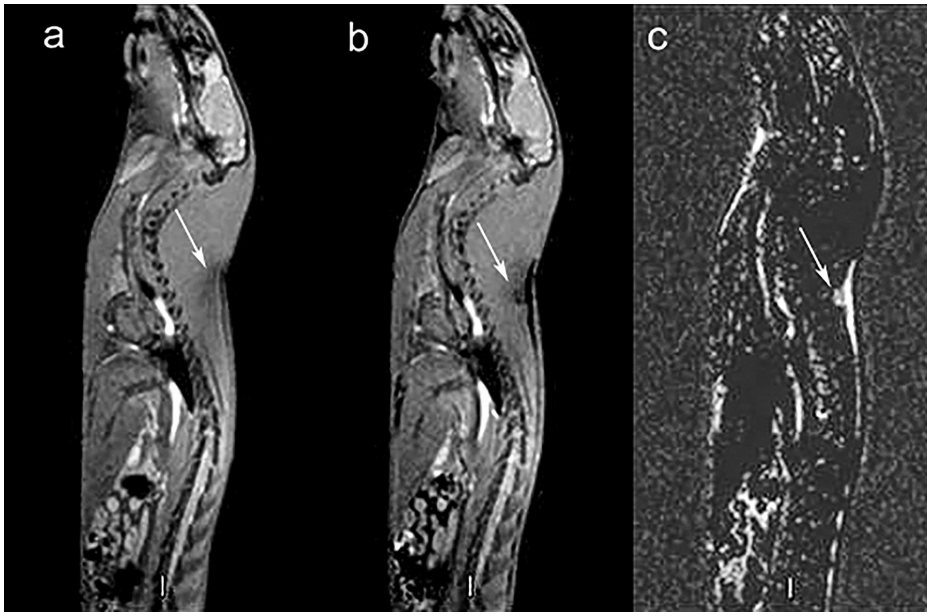

Figure 14. Interscapular brown adipose tissue (BAT) deposit in a rat. Sagittal in-phase (a), out-of-phase (b) and DUAL-SPIR (b) MR images depicting the interscapular brown adipose tissue (BAT) deposit in a rat. (c) is a calculated subtraction image acquired by subtracting the out-of-phase images from the in-phase images, which were obtained following a spectral presaturation inversion recovery (SPIR) pulse. Interscapular BAT in rats consists of a central mass and a bilateral butterfly-shaped area (arrow). As can be observed, the DUAL-SPIR subtraction method makes the BAT tissue distinguishable from the surrounding white adipose tissue, in contrast to in/opp imaging alone. Reprinted from study I.

6.2 DUAL-SPIR MRI IN HUMAN SUBJECTS (STUDY I)

Three healthy human volunteers were imaged as a part of the study. BAT could be outlined in DUAL-SPIR MRI subtraction ('fat-only') bilaterally in the cervical-supraclavicular area, but BAT was not as easily distinguished in humans as in rats. Metabolic activation of BAT was clearly visible in ^{18}FDG-PET/CT examination, visually corresponding excellently to DUAL-SPIR MRI.

Case 1 had 51 g of brown adipose tissue as measured by DUAL-SPIR MRI and 54 g as measured by ^{18}FDG-PET/CT. For cases 2 and 3, the amount of BAT measured with DUAL-SPIR MRI versus ^{18}FDG-PET/CT, was 32 g versus 46 g and 53 g versus 16 g, respectively.

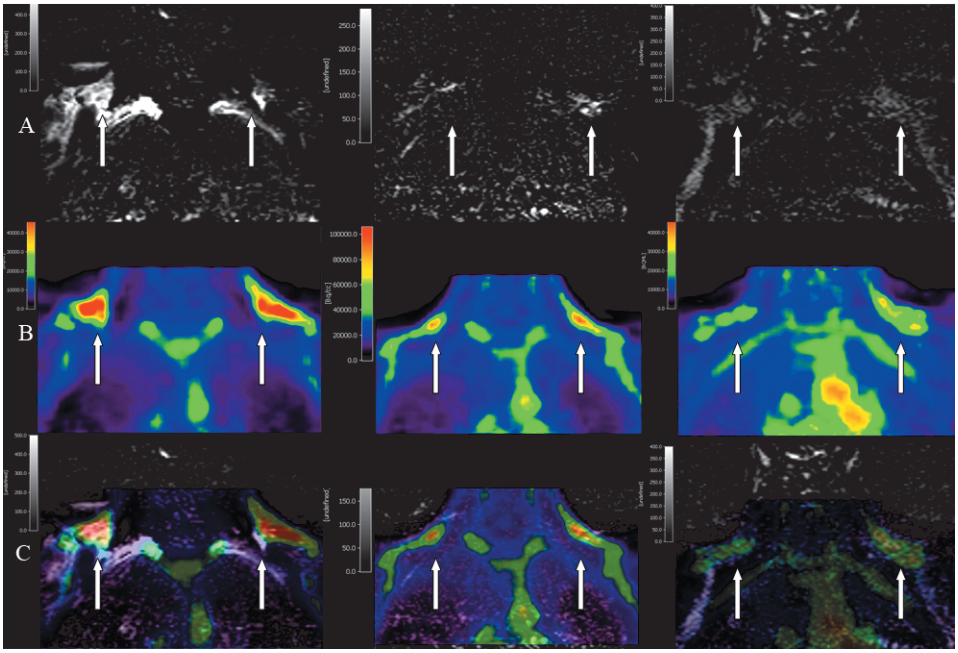

Figure 15. Human cases (study I). Calculated in/opp subtraction DUAL-SPIR images of the supraclavicular BAT deposits (arrow) in all 3 healthy human volunteers acquired in the coronal plane (a) and ^{18}FDG-PET/CT images (b) of the corresponding area in each subject. (c) is a fusion image of these MR and ^{18}FDG-PET/CT images. The actual amount of brown adipose tissue mass estimated by each technique is stated in the Results section. Reprinted from study I.

6.3 ^{1}H MRS COMPARED TO ^{18}FDG AND ^{15}O-H_2O PET (STUDY II)

^{1}H MRS showed the assumed BAT in the supraclavicular depot to contain both water and fat. The BAT triglyceride percentage varied between 60 and 91% (mean 77±10%

in all subjects, 71.5±9% in lean and 80.4±9% in obese subjects). Subcutaneous WAT contained significantly more triglycerides, 76-95% (mean: 87±5%, p=0.0002).

^{18}FDG-PET uptake in activated supraclavicular fat deposit tissue was compared between subjects with higher and lower than median levels of triglyceride content measured with ^{1}H MRS. No significant difference in cold-induced BAT activity between the high-triglyceride and low-triglyceride content groups was found. However, a tendency toward higher perfusion and glucose uptake in subjects with supraclavicular fat deposit triglyceride content above the median level was observed. ^{1}H MRS cannot be used for measuring volumes, due to the placement of single voxel inside the assumed BAT area.

6.4 HIGH BAT TRIGLYCERIDE CONTENT MEASURED BY ^{1}H MRS MAY BE A METABOLIC MARKER FOR DIABETES (STUDY II)

Subjects with below median value (78.1%) triglyceride content had higher M-values and HDL-cholesterol as well as lower fasting glucose level, BMI, waist circumference, waist-to-hip ratio and intra-abdominal fat mass, compared to those with higher than median values.

The triglyceride content in supraclavicular fat deposits correlated directly with weight, BMI, waist and hip circumference, intra-abdominal fat mass, and 8-year diabetes risk and inversely with HDL-cholesterol and M-value. The association between BAT triglyceride content and M-value remained significant independent of age, BMI, waist circumference and fat percentage. There was no correlation between triglyceride content in supraclavicular fat deposits and fat deposit perfusion measured with PET during cold exposure (r=-0.129, p=0.57).

The triglyceride content in supraclavicular fat deposits demonstrated a significant association with the log-transformed M-value when adjusted for waist circumference and age (β =-0.019 mg/kg/min, p=0.03), while the observed association for HDL-cholesterol was attenuated (β =-0.014 mmol/l, p=0.13). The supraclavicular fat deposit triglyceride content was associated with the log-transformed M-value (β =-0.025 mg/kg/min, p=0.01) when age and waist circumference were replaced with the Framingham diabetes risk score as the covariate.

6.5 ASSOCIATION BETWEEN BAT FAT CONTENT, T2* VALUES AND BAT GLUCOSE UPTAKE (STUDY III)

Cold-induced glucose uptake measured with ^{18}FDG-PET correlated with BAT SFF measured both during cold exposure (p = 0.02) and in ambient conditions (p = 0.02) as well as with BAT T2* relaxation time (p = 0.001 and p = 0.02, respectively). The areas with lower SFF (assumed to be BAT) in the supraclavicular fat depot could also be clearly detected visually. The values are seen in Table 2.

Table 2. Comparison of characteristics of subjects with low BAT triglyceride content (below the median level 78.1%) and high BAT triglyceride content (above median). Reprinted from study II supplementary appendix.

Characteristic (unit)	**below median triglyceride% n=11**	**above median triglyceride% n=11**	***p* value**
Age (years)	38,7±9.5	36,6±10.6	0.63
Weight (kg)	71.1±19.1	84.0±15.6	0.10
BMI (kg/m2)	25.6±6.7	30.4±5.8	0.09
Waist (cm)	***71.1±19.1***	***96.2±13.7***	***0.02***
Hip (cm)	98.0±16.4	106.4±13.5	0.20
Waist/Hip ratio	***0.81±0.07***	***0.90±0.07***	***0.005***
Systolic BP (mmHg)	116.0±11.7	121.9±15.6	0.33
Diastolic BP (mmHg)	72.8±8.2	74.6±10.0	0.65
Total cholesterol (mmol/l)	4.61±0.67	4.53±0.72	0.79
HDL-cholesterol (mmol/l)	***1.92±0.40***	***1.46±0.38***	***0.01***
LDL-cholesterol (mmol/l)	2.32±0.65	2.45±0.46	0.60
Triglycerides (mmol/l)	0.85±0.23	1.30±1.14	0.23
Intra-abdominal fat mass (kg)	***1.76±0.81***	***2.75±1.10***	***0.04***
Subcutaneous fat mass (kg)	7.37±7.21	8.58±5.13	0.67
WAT fat percentage (%)	86.4±5.0	88.0±4.6	0.48
Body fat percentage (%)	34.2±9.1	37.6±11.3	0.44
Log-transformed M-value (mg/kg/min)	***3.81±0.30***	***3.15±0.36***	***0.0002***
OGTT 2-hour glucose (mmol/l)	6.13±0.93	6.76±1.08	0.15
OGTT glucose AUC 0-120 minutes (mmol/l*min)	871.2±119.2	918.4±126.7	0.379
Fasting glucose (mmol/l)	***5.06±0.27***	***5.33±0.29***	***0.04***
BAT ^{18}FDG uptake during cold exposure	6.08±5,22	6.98±7,21	0.74
BAT perfusion during cold exposure	12.4±8.33	10.9±4.60	0.61

6.6 EFFECTS OF COLD EXPOSURE ON MRI RESULTS (STUDY III)

T2* and SFF studies were performed during cold exposure and in ambient conditions. Regardless of cold exposure, the measurements showed a supraclavicular BAT depot containing water and fat, with significantly lower SFF and T2* time compared to subcutaneous WAT (SFF versus WAT and T2* versus WAT both $p < 0.0001$ during cold exposure and at ambient temperature). The SFF of muscle was low and the T2* relaxation time higher compared to BAT, and these values did not change with cold exposure. The values are seen in Table 3.

Cold exposure did not significantly change the SFF or T2* in BAT, WAT or muscle. (for SFF p= 0.62, 0.51 and 0.40, and for T2* p=0.31, 0.38 and 0.36, respectively).

Table 3. SFF and T2* relaxation time values in BAT, WAT and muscle during cold exposure and in ambient conditions. Modified and reprinted from study III.

Characteristic (unit)	**Mean**	**Correlation to BAT glucose uptake**	
		***r* value**	***p* value**
BAT SFF during cold exposure (%)	**81.9 ± 4.0**	**-0.64**	**0.02**
BAT SFF at ambient temperature (%)	**82.3 ± 3.8**	**-0.63**	**0.02**
WAT SFF during cold exposure (%)	90.0 ± 2.9	0.06	0.84
WAT SFF at ambient temperature (%)	89.1 ± 3.2	0.10	0.75
Muscle SFF during cold exposure (%)	6.7 ± 1.4	-0.29	0.33
Muscle SFF at ambient temperature (%)	7.6 ± 2.4	-0.18	0.55
BAT T2* relaxation time during cold exposure (ms)	**15.3 ± 1.1**	**-0.79**	**0.001**
BAT T2* relaxation time at ambient temperature (ms)	**14.8 ± 1.8**	**-0.65**	**0.02**
WAT T2* relaxation time during cold exposure (ms)	20.7 ± 2.0	0.20	0.52
WAT T2* relaxation time at ambient temperature (ms)	20.4 ± 1.4	0.26	0.38
Muscle T2* relaxation time during cold exposure (ms)	28.6 ± 3.4	-0.12	0.70
Muscle T2* relaxation time at ambient temperature (ms)	25.6 ± 3.4	-0.01	0.98

7 DISCUSSION

The first design for this research was drafted in 2008. During that time, the now well-known studies confirming the existence of BAT on healthy adults had not been published (Cypess et al. 2009; van Marken Lichtenbelt et al. 2009; Virtanen et al. 2009). There was very little literature about MR imaging of BAT on rodents (Sbarbati et al. 1997; Lunati et al. 1999). On humans, there were only some case reports on hibernomas, rare lipomatous tumors containing BAT (Anderson et al. 2001; Baldi et al. 2004), and one case of a paraneoplastic syndrome resulting in BAT expression on a patient with adrenal pheochromocytoma (Dundamadappa et al. 2007).

As a consequence of the use of ^{18}FDG-PET on oncological purposes to trace tumor metastases, BAT started to emerge as an incidental and often confounding finding in clinical ^{18}FDG-PET examinations (Nedergaard, Bengtsson, and Cannon 2007). At first it seemed that ^{18}FDG-PET would be the modality of choice for research of BAT, too. From the radiological perspective, MRI seemed to be a modality well suited for assessment of a tissue with both fat and water, as well as different amounts of iron compared to surrounding tissues.

The first goal for this research was to confirm that BAT could be detected with MRI (Study I). The sequence combined two common methods to separate the tissue MR signal into its fat and water components (in/opp imaging and SPIR). In retrospect, it was heavily dependent on the scanner properties, and as thus, not easily reproducible. It was designed for purely visual detection of BAT from WAT, and could not be used for numerical estimations of triglyceride content. However, it decidedly confirmed the capability of MRI in the detection of BAT, and it was one of the first MRI studies including human subjects. At that time the images of visual comparison of ^{18}FDG-PET activation and DUAL-SPIR were quite impressive, and the study was one small milestone on the way of developing in/opp sequences for BAT research.

Since then, several methods for investigating BAT on MRI have been proposed and studied in the scientific literature, with varying imaging conditions and circumstances. This study has engaged in testing MRI sequences, comparing them with other MR sequences, ^{18}FDG-PET activation, clinical parameters and biopsies(Studies II, III). The effect of cold exposure on MRI examinations has been investigated, and the study also participated in demonstrating the possible clinical significance of BAT as a biomarker (Study II). The advancements on this field have been immense during these 10 years, and we have been proud that we have been a small part of this research community.

7.1 DEVELOPING DIXON-BASED IMAGING SEQUENCES FOR BAT STUDIES (STUDY I)

In study I, MRI was shown to be able to unequivocally demonstrate the presence of BAT on rats. An in/opp sequence was used, both with and without fat suppression (SPIR). The subtracted sequence first utilized in the study I for evaluating BAT is calculated from in/opp MR images by subtracting the signal of the out-of-phase image from the in-phase image, producing a fat-only image. The sequence was modified by adding a fat suppression pulse (SPIR) before imaging, with otherwise similar postprocessing, resulting in a fat-suppressed fat-only image.

The higher water content of BAT results in greater signal cancellation on standard out-of-phase images compared to that of WAT. The addition of a fat selective suppression pulse decreases the amount of phase cancellation and in theory this could have made the technique less sensitive to differences in tissue water content. We hypothesized that the SPIR pulse suppressing the fat signal in DUAL-SPIR would measure changes that are occurring in the water component of the signal, instead of fat.

This sequence distinguished BAT tissue from WAT visually well in a rat model. However, in human subjects, the sequence proved to be unreliable, possibly partly due to the unpredictable results of fat suppression on different scanners and on an artifact-prone area, and partly due to the fact that in adult humans BAT is recruitable 'brite' fat instead of true BAT, a mixture of brown and white adipose cells in different stages of transdifferentiation, and thus the water content is smaller and more variable than in true rodent BAT. In addition, although visually the contrast between BAT and WAT was good and the existence and volume of BAT could be discerned, the sequence did not yield actual measurable values for comparison purposes.

There are some concerns regarding the imaging procedure. Because the rats were euthanized with CO_2 prior to the MRI studies, the blood concentration of deoxyhemoglobin was likely higher than on living animals. This may have shortened the T2* of BAT relative to WAT, since BAT has substantially greater capillary volume compared to WAT. The shorter T2* decay may have produced a greater difference in signal intensity between the 2.3 ms (in-phase) and 4.6 ms (out-of-phase) images. While the study was not intended to determine the mechanism of contrast, it is possible that the results presented might have been different on living animals, with the blood oxygenation level contrast (BOLD effect) likely to be smaller. There was no substudy involving anesthetized rats. However, the DUAL-SPIR imaging contrast on human subjects with normal blood oxygen levels seemed to be sufficient, suggesting the effect of deoxyhemoglobin to not to be substantial.

After study I was published, other methods of postprocessing Dixon images were presented to obtain values that could be more easily compared. Different ratios were calculated, for example a water-to-fat signal ratio (Chen et al. 2013). Subsequently the technique was further refined by dividing the fat-only image with the in-phase image, producing a signal-fat-fraction (SFF) image, a commercial sequence now widely used in BAT imaging (Hu, Yin, et al. 2013; Franz et al. 2015; Deng et al. 2015). Nonetheless, our research did prove the feasibility of Dixon-based MRI in examining BAT and paved the way for more advanced postprocessing techniques.

Study III continued with the feasibility studies of Dixon imaging using the SFF technique with commercially available standardized sequence, concentrating on the effects of cold exposure.

7.2 BAT FAT CONTENT, T2* VALUES AND PET GLUCOSE UPTAKE (STUDY III)

The SFF values measured in our study were slightly higher than in previous studies conducted on younger populations (Hu, Perkins, et al. 2013), but later research has reaffirmed our results in adults using the same SFF technique (Deng et al. 2017; Franssens et al. 2016; Franssens et al. 2017). SFF is a robust technique for measuring fat and water content and thus determining the existence and volume of BAT. The results produced with the standardized commercial sequence are also easily comparable.

In our study, the T2* values were in line with previous findings (Hu, Perkins, et al. 2013; Hu, Yin, et al. 2013), considering that the age of the subjects was different. T2* mapping as a technique has not been applied to BAT imaging as frequently as SFF, and there are no available commercial sequences or postprocessing software adapted to BAT. As a result, the method still lacks standardization, the scanner parameters being subtly different, making the comparison of the values difficult. T2* mapping is an intriguing potential technique for the dynamic assessment of BAT, but more research is still required to achieve a robust and dependable sequence and postprocessing method for routine use. Study III was part of this ongoing research.

No correlation of BAT ^{18}FDG uptake, SFF or T2* values with age or BMI was found in this study. The reason may be that the number of volunteers was relatively small, and there was only minor variation in the weight and age of the subjects. It is possible that correlation could be found with a larger and more heterogeneous group of volunteers. A later study specifically engineered to include young men with diverse BMI showed obese subjects to have higher SFF than nonobese subjects both under cold exposure and in ambient conditions, but there were no correlations between

MRI measurements and PET/CT measurements of BAT (Deng et al. 2017). To date, there seems to be no such data assessing the correlation between MRI measurements of BAT and age. In previous literature, the amount of activated BAT measured by ^{18}FDG-PET has been shown to inversely correlate with both age and BMI (Saito et al. 2009; Stahl et al. 2016; Virtanen et al. 2009; Yoneshiro et al. 2011).

In a recent study, it was found that obese young men had less activated BAT than lean men but more fat in BAT-containing depots (Leitner et al. 2017). This suggests that the activation state of BAT might be more important than the existence of anatomical BAT, accentuating the demand for different methods and perspectives on BAT research.

SFF mapping, T2* mapping, and ^{18}FDG uptake all seem to assess different aspects of BAT. It is likely that by combining these techniques, the identification of BAT can be improved. This is especially beneficial when utilizing SFF and T2* mapping, since these measurements can be acquired simultaneously. The differences between WAT and BAT in the fat and water content as well as in oxygen consumption, iron content and perfusion properties can be assessed using sequences that measure synchronously SFF, T2 relaxation and T2* relaxation. Algorithms such as those based on thresholding, region-growing, watershed, active contours and neural networks may be able to better utilize this extensive amount of data. There are already preliminary studies on animal data (Bhanu Prakash et al. 2016). In the future it is very likely that combination of different MRI data and maybe even data from different modalities can be employed using computer algorithms and machine learning.

7.3 THE ROLE OF COLD EXPOSURE ON SFF AND T2* MAPPING (STUDY III)

^{18}FDG-PET has been the gold standard in detecting BAT in humans (Cypess et al. 2009; Saito et al. 2009; van Marken Lichtenbelt et al. 2009; Virtanen et al. 2009). It is a functional imaging modality, requiring metabolic activation through cold exposure, which is a lengthy procedure and a source of significant discomfort for the subjects. This limits the routine use of the technique for clinical purposes or larger-scale research.

In early human research on BAT conducted with MRI no cold exposure was utilized (Chen et al. 2013; Franz et al. 2015; Hu, Perkins, et al. 2013; Hu, Yin, et al. 2013). It was hypothesized that BAT activation would not have a significant effect on the anatomical fat composure assessed by MRI. This assumption was questioned, when Chen et al. applied BOLD fMRI to imaging BAT (Chen et al. 2013), while van Rooijen et al. used dynamic T2*-weighted MRI revealing signal fluctuations that were assumed to be associated with BAT activation (van Rooijen et al. 2013), both during

mild cold challenge. Romu et al. examined the effect of longer-term cold exposure on MR Dixon imaging in an animal model, demonstrating rat BAT volume to increase and SFF to decrease after 5 days of cold challenge (Romu et al. 2015).

The first Dixon MRI studies during acute cold exposure in human BAT showed the BAT SFF to slightly decrease, suggesting either increased perfusion or lipid consumption (Lundstrom et al. 2015; Stahl et al. 2016). In contrast to the aforementioned studies, no significant effect of cold exposure on MRI properties was found in the present study. The temperature changes had no measurable effect on the SFF values. T2* relaxation times were slightly elevated during cold exposure in both BAT and WAT, but the change was not significant.

The imaging protocol used in this study differed considerably from the previous studies. A 3D VOI was semiautomatically drawn on SFF images including the whole supraclavicular fat depot. The resulting 3D VOI was reduced twice in size using the automatic shrink option, to avoid possible contamination of nearby tissues resulting from chemical shift artifacts (MRI), spillover effect (PET) or small motion artifacts. Avoiding contamination by muscles and vascular structures is crucial for acquiring accurate measurements for BAT.

Despite this rigorous shrinking, the VOIs in our MR sequences were still about 20-fold in volume compared to some studies with minuscule VOIs containing only maximally activated BAT (Stahl et al. 2016). BAT consists of brown and white adipocytes at different stages of differentiation, and our method examines the whole volume of this possible beige fat, not only the strongest activation. It is conceivable that averaging effect may diminish small differences in SFF in larger VOI volumes. In the present research we also fastidiously confirmed our VOI to include only fat tissue, with no contamination by muscles or blood vessels. In some studies, the fat segmentation is less rigorous and seems to include vascular structures, increasing the perfusion effect (van Rooijen et al. 2013). Due to the differences in the definition and segmentation of the BAT tissue it is difficult to compare this research to previous literature.

In conclusion, depending on the setting, cold exposure may not be necessary with MR imaging. Anatomical fat imaging can certainly be performed without cold conditioning, confirming the existence and quantifying the volume of BAT. According to our study, for this purpose, SFF mapping and T2* mapping seem to be able to assess BAT independent of the activation state of the tissue. The fine changes in cold-activated BAT detected by dynamic MR imaging in recent studies are likely caused by lipid consumption and/or increased blood flow (Lundstrom et al. 2015; van Rooijen et al. 2013). They are considerably smaller than the differences between BAT and WAT recorded in our study. They still mean that BAT activation can probably be

examined by dynamic MRI studies. For this purpose, further research is needed to produce MR sequences that are both sensitive and robust.

7.4 BAT TRIGLYCERIDE CONTENT AS A METABOLIC MARKER (STUDY II)

The feasibility of using the ^{1}H MRS protocol to investigate BAT triglyceride content was tested in study II. It was used to examine a population of both lean and obese volunteers. In this study, we were the first to demonstrate that high BAT triglyceride content measured by ^{1}H MRS may be independent risk factor for diabetes.

According to our findings, the measurement of supraclavicular fat deposit triglyceride content could identify healthy subjects at increased risk of developing insulin resistance independent of obesity. Supraclavicular fat deposit triglyceride content correlated directly with obesity markers (e.g., BMI, waist and hip circumference, intra-abdominal fat mass) and inversely with HDL-cholesterol and whole-body insulin sensitivity as measured by the M-value. The inverse association between insulin sensitivity and supraclavicular fat deposit triglyceride content was independent of age, BMI, waist circumference, or 8-year risk of diabetes (as estimated by Framingham risk score), suggesting BAT may have a role in the pathogenesis of insulin resistance independent of conventional diabetes risk factors. In line with these findings, it was later demonstrated that the increase of the BAT triglyceride content in the supraclavicular fat depot can influence the development of insulin resistance in patients with DM2 and prediabetes (Koksharova et al. 2017, Chondronikola et al. 2016)

The novel finding in this study suggesting BAT triglyceride content being an independent mediator of whole-body insulin sensitivity independent of BAT metabolic activation, is well in line with a study pointing toward a protective effect of BAT presence in age-associated development of obesity in humans (Yoneshiro et al. 2011), as well as with research suggesting the existence of BAT to be independently associated with BMI, body fat mass and abdominal visceral and subcutaneous fat areas, acting as an independent determinant of glucose and HbA1C (Matsushita et al. 2014).

Causality between BAT triglyceride content, obesity, and insulin sensitivity could not be proven, since the study design was cross-sectional. BAT could function as an adipose organ with independent high glucose uptake or BAT activity may be a marker for insulin sensitivity in other tissues. Fatty infiltration of various tissues is a major player in the development and progression of obesity and diabetes. It is possible that this increase in BAT triglyceride content shares similar pathogenesis with other factors in metabolic syndrome, such as the accumulation of fat tissue and fatty

infiltration of the liver and pancreas. In the present study, intra-abdominal fat depots were 56% larger in patients with a lower than median BAT triglyceride percentage. The liver or pancreas triglyceride content was not measured.

Recently, lower BAT triglyceride content measured with SFF maps has also been shown to associate with less obesity and a more favorable metabolic profile in patients with clinical manifest cardiovascular disease (Franssens et al. 2017). This seems to suggest that albeit ^{1}H MRS is the most exact method for measuring the triglyceride content in vivo, SFF would be accurate enough to be used for this same purpose. It also has the added benefit of better anatomical resolution and the possibility for dynamic acquisition.

In conclusion, the triglyceride content in supraclavicular fat deposits may be an independent marker of whole-body insulin sensitivity, independent of BAT metabolic activation. Possible underlying mechanisms are independent high glucose uptake or BAT activity being an indirect metabolic marker for insulin sensitivity in other tissues. More studies are needed to establish the relationship between changes in BAT triglyceride content and glucose metabolism, in patients with metabolic syndrome and T2DM. The current findings confirm the growing opinion that BAT can be seen as a whole-body barometer of metabolic health.

7.5 ROLE OF MRI AND ^{1}H MRS IN BAT STUDIES (STUDIES I - III)

MR-based techniques, such as ^{1}H MRS, SFF and T2* mapping are safe and reliable methods for identifying BAT and measuring its triglyceride content, with no associated radiation burden.

^{1}H MRS and SFF imaging have the benefit of producing percentage measurements of triglyceride content. SFF excels in accurate anatomical imaging, while ^{1}H MRS is the most exact method for assessing triglyceride content in vivo. This study emphasized that different MR sequences and ^{1}H MRS have great synergy when performed together, allowing for simultaneous assessment of the anatomy and fat content. According to recent research, along with fat fraction, temperature can also be derived from ^{1}H MR spectra providing further tools to estimate BAT activation (Koskensalo et al. 2017).

SFF mapping (Lundstrom et al. 2015) and T2*mapping (van Rooijen et al. 2013) can possibly be used to assess the rapid changes in perfusion and lipid consumption during cold-induced activation of BAT. Thus far, ^{18}FDG-PET has been the gold standard in the dynamic acquisition of BAT activity, but this will likely be challenged in the future with emerging safe and noninvasive MRI methods.

Despite all the research on the association of BAT volume and function in obesity and metabolic syndrome, there is currently no clear indication for the imaging of BAT in clinical practice. There are already commercial sequences for SFF mapping that are easy to utilize. However, the actual imaging and consequent data analysis of T2* mapping and ^{1}H MRS require a certain level of skill and training, and this reduces the speed of the possible clinical implementation of these techniques. However, with possible obesity-related interventions and medications in the future, clinical imaging and the subsequent implementation of automated routines by MR device manufactures is expected.

Thus far, ^{18}FDG-PET has been the noninvasive gold standard for BAT measurement. It is a robust and well-researched method, but has several disadvantages. The radiation burden is considerable. This is emphasized by the need for the recurrent imaging of healthy volunteers, making safety an important concern. ^{18}FDG-PET imaging also requires the activation of BAT by cold exposure, which is a lengthy and inconvenient procedure for the volunteers. The easier availability and lower cost of MRI should also be considered as a benefit for research protocols.

According to this research, MRI is the recommended modality for confirming the existence of BAT and measuring BAT volume, while both ^{1}H MRS and SFF excel at assessing tissue triglyceride content. There is already some research on using dynamic MRI to investigate BAT activation, but PET is still vastly better researched on this subject. In the future it is likely that MR techniques, including SFF, T2*mapping and ^{1}H MRS, will have a greater role in BAT research due to their easier availability and lack of radiation exposure.

7.6 STRENGTHS AND LIMITATIONS

In this study, BAT has been investigated comprehensively and from different angles. It has been examined in an animal model, in healthy volunteers and in obese people. MR imaging (both Dixon-based techniques and T2* mapping), ^{1}H MRS, and ^{18}FDG-PET have been used, after cold exposure as well as in ambient conditions, comparing the results. The clinical relevance of triglyceride content in BAT as a possible independent marker of whole-body insulin sensitivity has also been demonstrated. To the best of our knowledge, there are no previous studies which have compared MR properties and ^{18}FDG-PET activation of BAT this extensively and thoroughly.

The number of all volunteers was satisfactory in the whole study, although the study groups could have been more heterogeneous. Most of the subjects were healthy, of normal weight, and aged 20–40 years. No children or elderly people were included. Only in study II was there variability in the measured BAT triglyceride content in our material. Including people with more diverse backgrounds and especially more

subjects with obesity and metabolic syndrome might have given more distinct results. Thus, further evaluation in a larger number of patients is required. This study did include prospective and novel data in addition to cross-sectional and validation studies, which are considered more reliable than retrospective studies. Accordingly, a larger prospective study or pooled data of multiple studies is required to draw conclusions on the specific MR properties of BAT.

The supraclavicular depot being an artifact-prone area, the imaging sequences for BAT need to be robust, while simultaneously better spatial and temporal resolution are needed. The reproducibility and robustness of T2* mapping in particular needs to be validated. To date, there are no viable commercial solutions for easy and precise measurements of T2* values.

7.7 FUTURE CONSIDERATIONS

Research on the causes and consequences of metabolic syndrome is urgently needed in the near future. The properties of adipose tissue, including BAT, are attracting tremendous interest. Adipose tissue is no longer considered to be a simple and passive energy depot, but a central node in multi-directional organ cross-talk. ^{1}H MRS and MRI are both powerful tools for evaluating and quantifying fat. In the future, real-time activation of both BAT and WAT will probably play a larger role in research. New and improved imaging techniques will also be in demand.

More validation of existing MR techniques will be needed. Larger, controlled trials are required particularly in this regard. Fortuitously, MRI as a modality is noninvasive and has no radiation burden. This renders repeated examinations of healthy volunteers safe.

3T scanners are increasingly used in clinical practice. The higher field strength has known advantages, such as faster acquisition time, but it is also more sensitive to susceptibility and motion artifacts. The availability of MRI will improve rapidly in the future, enabling easier opportunities for both research and possible clinical applications of fat tissue MRI. However, clinical indications for this are yet to be determined. Easy commercial sequences and solutions for the functional examination of adipose tissue will also be needed before routine assessment is conceivable.

In terms of next-generation perfusion imaging, there are some interesting experimental techniques such as vessel architectural imaging (Emblem et al. 2013), which measures microcirculation, oxygen saturation, and vessel caliber using a combination of readout-segmented echo-planar imaging (EPI), and parallel imaging, noninvasively without the use of a contrast agent. This approach provides a robust

correction for motion-induced phase artifacts and allows scan times that are suitable for routine clinical application (Porter and Heidemann 2009). To our knowledge, vessel architectural imaging has not been performed on BAT, and this would be an interesting application for noninvasive dynamic BAT imaging.

In conclusion, ^{1}H MRS and MRI are safe and noninvasive modalities for evaluating and quantifying both WAT and BAT. They are able to assess both triglyceride content and volume of fat tissue unequivocally. In the future, this provides the means to combat increasing worldwide obesity and metabolic syndrome by providing more information on this fascinating and vital component of body metabolism.

8 CONCLUSIONS

The conclusions of this study are:

I BAT can be unequivocally detected using MR imaging. Dixon method-based MRI applications, such as SFF, seem to be a superior method for assessing tissue volume. BAT triglyceride content as a marker for metabolic activity can be measured with SFF and proton spectroscopy (^{1}H-MRS). (Studies I-III)

II ^{1}H MRS can be used to assess BAT and WAT triglyceride content. Triglyceride content in BAT may be an independent metabolic marker of whole-body insulin sensitivity. (Study II)

III Cold exposure does not seem to have a considerable effect on SFF and T2* measurements. (Study III)

IV MRI is superior to PET imaging while examining BAT volume, due to the excellent tissue contrast, noninvasiveness and lack of radiation burden. (Studies I – III)

ACKNOWLEDGEMENTS

This study was carried out at the Turku PET Centre, University of Turku, the Medical Imaging Centre of Southwest Finland, Turku University Hospital, and the Department of Radiology, University of Turku during the years 2009-2018. It was financially supported by the European Union, as well as grants from Turku University Hospital, University of Turku and the National Graduate School of Clinical Investigation.

I want to warmly thank all those who have encouraged and helped me during these years.

I am grateful to Professor Juhani Knuuti, director of the Turku PET Centre, for providing the excellent facilities for my research. I also wish to express my gratitude to Professor Hannu Aronen for his support of research as well as for his all-encompassing love of science and radiology.

I owe my sincere gratitude to all my supervisors, Docents Riitta Parkkola, Pirjo Nuutila and Ronald Borra for their continuous support and encouragement.

Dear Riitta: Thank you for encouraging me over and over again, and for setting an example of an outstanding researcher, colleague and radiologist. Your positive attitude and sheer power of personality kept me continuing the research even on the days I felt sceptical of the process. You are my role model in so many ways. I also thank you for your tremendous help on writing and publishing the articles - your experience and hard work made this possible!

Dear Pirjo: Working with you has been a great privilege. Your vast experience, knowledge and practical approach have kept me in check. You have established order and logic in my research, and taught the value of hard work. When I faced challenges, you taught me to take one step at a time, and every single piece of advice has been solid and appreciated. Thank you for teaching me and always supporting me.

Dear Ronald: I really look up to the way you seem to understand and love nuclear physics and imaging. You have installed in me a curiosity and love towards MR imaging. You manage to explain even the complicated details so that I understand, and your help has been invaluable in designing this research.

I wish to thank the official reviewers, Assistant Professor Vera Schrauwen-Hinderling and Adjunct Professor Kirsi Timonen for all their time and effort during the review of this work. Their thorough and constructive comments have improved this thesis enormously. My thanks also to all of the anonymous reviewers of the original publications for their feedback.

I wish to thank Docent Kirsi Virtanen for her patience with me. Her tremendous experience and knowledge of all the aspects of brown adipose tissue have provided me an outstanding environment for starting my research, when I was completely inexperienced.

I am extremely grateful to all the outstanding physicists who have helped me during the research: Markku Komu, Marko Pesola, Jani Saunavaara, Virva Saunavaara, and Kalle Koskensalo. Thank you so much for all your time, effort and never-ending patience! You have always provided insightful answers to all my naive questions, explaining kindly (and repeatedly) the principles and particulars of MRI. I truly admire how you can devise numbers and parameters where I see images. I also wish to thank Professor Mika Teräs for the kind support and the interest in my thesis.

I wish to thank Dr. Juho Raiko for his patience in co-authoring those articles with me. I am very grateful for his clinical experience and especially for all the help with the statistics! I also want to extend my thanks to Teemu Saari and Janne Orava for their efforts in analyzing the PET data, and especially teaching me the important details of how to meticulously draw the VOIs.

I have felt privileged to work with all of my excellent co-authors. I want to thank Tove Grönroos for her excellent work with the PET imaging on the animal model, Jukka Laine for his outstanding histological analyses of the biopsies, Tarja Niemi for her expertise in performing the biopsies on difficult supraclavicular area, and Markku Taittonen for performing the anesthesia. I also want to thank the biostatisticians, Irina Lisinen and Jaakko Matomäki, for their outstanding advice on statistical methods and for performing many essential statistical analyses in this work.

My deepest appreciation goes to the remarkably skilled MR and PET technologists in the Turku Pet Centre, as well as for all the assisting personnel. I am particularly grateful for the assistance given by the research coordinating nurse Mia Koutu.

I cannot laud enough the significance of the patients and healthy volunteers who chose to participate in this study. Their participation has made this work possible and I am very grateful for their patience during the long PET and MR-scanning sessions, not to speak of the cold exposure, which they endured better than I could have expected.

I wish to thank the guidance group, who trusted me to advance my research, even if it at times seemed to go slowly. Thank you Docent Kimmo Mattila, Professor Juha Rinne and Docent Helena Lapinleimu.

I wish to express my gratitude to the Chairman of the Medical Imaging Centre of Southwest Finland, Roberto Blanco Sequeiros, for giving me the opportunity to engage in research regardless of the extensive workload in the clinic. He has also encouraged me to widen my perspective and provided me with the chance to improve my knowledge of radiology, both in Finland and in institutes abroad.

I am thankful for Assistant Chief of the Department of the Radiology, Sakari Salo, as well as the former Chairmen, Adjunct professor Anu Alanen and Juha Sjövall, for their support. I am truly thankful to Jaana Keihäs and Pirjo Helanko, for their professional and kind secretarial help. Special thanks to Jaana, for always knowing the answer for every conceivable bureaucratic problem.

I have been privileged to work with the best colleague I could ever have, Ia Kohonen. She has encouraged me in my research, even if it has meant more clinical workload for her. The fact that she so effortlessly and professionally defended her dissertation a year ago encouraged me to finish this thesis. She is a role model for me – I admire her kind and patient presence and uncompromising work ethic, while still maintaining a lovely sense of humor.

I owe my sincere thanks to Docent Kimmo Mattila. I am honoured to have him as my mentor on my path to a musculoskeletal radiologist. He has always been watching over me, helping when needed but also providing me with the opportunity to start spreading my own wings. His constant guidance has been an enormous assurance for me and I hope he will keep an eye on me in the future, too.

I want to also thank Ville Armio, a friend and a colleague whose unbridled enthusiasm towards imaging and radiology always motivates me. He keeps reminding me why musculoskeletal radiology is so much fun!

There are no words to describe how grateful I am for my colleagues in the Department of Radiology in Turku University Hospital. Pirkko Sonninen, for her compassion and professionalism; Jari Karhu and Teemu Paavilainen, for their terrible sense of humor, for which I just always seem to fall; the lovely radiologist ladies Ilona Koski, Johanna Virtanen, Satu Päivike, Minna Sandell, Susanna Pekanheimo, Laura Nummijärvi, Carita Kovio and Aida Kiviniemi for their company on many excursions for professional and fun purposes; Jussi Hirvonen for the shared interest in the future of radiology, by employing the cutting edge technology and teaching the new generation; Jussi Kankare, for his jovial, no-nonsense attitude; Maitta Hartikainen, for her personality and spirit; and Professor Peter Dean, who has been a great example for all of us, both in his interest in science and in his friendly and encouraging attitude. I really love the easy-going, encouraging spirit and delightful conversations in our department. The bright and enthusiastic younger colleagues truly remind me why I love radiology, and the more experienced colleagues teach me more about radiology and life every day.

I am deeply grateful for the skilled radiographers with whom I have the privilege to work with, in A-röntgen, T4-röntgen, T2-röntgen, ER department röntgen, TKS-röntgen, U-röntgen and the regional röntgen departments. Special thanks to Mira Hallenberg for the technical help with the cover image!

I have been fortunate to work daily with skillful and competent doctors in Turku University Hospital. Especially I want to thank my orthopedic surgeon and reumathologist colleagues, as well as the members of the Turku Sarcoma Group. Your talent and knowledge are an inspiration to me, and I try to provide you with the same level of the professionalism you continuously show.

I am deeply grateful for the continuous support and confidence from my friends. Our very scientific lunch meetings with my friends and fellow researchers Sanni Kotimäki and Reetta-Liina Armio have provided a necessary break during the writing process, and occasionally I have even burdened them with the details and statistics. I want to thank Jenni Janatuinen, with whom I have experienced so much together since medical school, as well as Laura and Lauri Tanner for our long friendship and shared memories. I am thankful to everyone I have studied with in Turku Medical University – I still see so many of them at work every day, and I really feel a sense of community here.

I owe my sincere thanks to my geeky friend group, with whom we meet regularly – especially Leea, Elina, Mari and Alia. I also appreciate immensely Conviction, and all the friends I made during those years; I learned teamwork and leadership, which have helped me immensely later on. I really appreciate my dear samba friends in Finland and abroad, for maintaining my mental and physical condition (well, they are stable at least).

I truly love my siblings Jukka, Sirkku and Topi (and also Janne, who is forever my brother even if he is no longer with us). They all have families, and I am so proud of the young generation, every single one of them. Especially I adore my nieces: smart and sassy Vilma, who will conquer the world, as well as lovely and compassionate Johanna, who goes out of her way to save the world.

I express my deepest gratitude to my dear parents, Marja and Aki Lusenius, for always encouraging me to take interest in the world and to search for more knowledge. You have always made me believe that my opinions matter, and I have been able to discuss everything with you. Mum, you have been an example for me on how to teach with enthusiasm, interest and genuine compassion, and I really admire how you have always been ready to fight for equality and justice. And dad, your practical help in numerous situations has been crucial. You have also encouraged me with the research, and in the end the writing process of my thesis proved to be shorter than the process to get Carthago destroyed.

Above all, dear Tero, my husband and best friend – my deepest thanks for enduring me all these years. I thank you for your pragmatic and objective views, help and support and also for the patience, persistence and encouragement. I love your sense of humor, your quiet strength and your constant aspiration for fairness. You are the most important person for me in this world.

REFERENCES

Ahmadi, Naser, Fereshteh Hajsadeghi, Mark Conneely, Mark Mingos, Rohit Arora, Matthew Budoff, and Ramin Ebrahimi. 2013. 'Accurate Detection of Metabolically Active Brown and White Adipose Tissues with Computed Tomography', *Academic Radiology*, 20: 1443-47.

Anderson, S.E., C. Schwab, E. Stauffer, A. Banic, and L.S. Steinbach. 2001. 'Hibernoma: imaging characteristics of a rare benign soft tissue tumor', *Skeletal Radiol*, 30: 590-95.

Baldi, A., M. Santini, P. Mellone, V. Esposito, A.M. Groeger, M. Caputi, and F. Baldi. 2004. 'Mediastinal hibernoma: a case report', *J. Clin. Pathol*, 57: 993-94.

Bhanu Prakash, K. N., S. K. Verma, J. Yaligar, J. Goggi, V. Gopalan, S. S. Lee, X. Tian, S. Sugii, M. K. Leow, K. Bhakoo, and S. S. Velan. 2016. 'Segmentation and characterization of interscapular brown adipose tissue in rats by multi-parametric magnetic resonance imaging', *MAGMA*, 29: 277-86.

Bitar, R., G. Leung, R. Perng, S. Tadros, A.R. Moody, J. Sarrazin, C. McGregor, M. Christakis, S. Symons, A. Nelson, and T.P. Roberts. 2006. 'MR pulse sequences: what every radiologist wants to know but is afraid to ask', *Radiographics*, 26: 513-37.

Bloch, F. 1946. 'Nuclear Induction', *Physical Review*, 70: 460-74.

Bloembergen, N., E. M. Purcell, and R. V. Pound. 1948. 'Relaxation Effects in Nuclear Magnetic Resonance Absorption', *Physical Review*, 73: 679-712.

Borra, R., R. Lautamaki, R. Parkkola, M. Komu, P.E. Sijens, K. Hallsten, J. Bergman, P. Iozzo, and P. Nuutila. 2008. 'Inverse association between liver fat content and hepatic glucose uptake in patients with type 2 diabetes mellitus', *Metabolism*, 57: 1445-51.

Bosello, O., and M. Zamboni. 2000. 'Visceral obesity and metabolic syndrome', *Obes. Rev*, 1: 47-56.

Bottomley, Paul A, and John R Griffiths (ed.)^(eds.). 2016. Handbook of Magnetic Resonance Spectroscopy In Vivo: MRS Theory, Practice and Applications (Wiley).

Cernea, S., and M. Dobreanu. 2013. 'Diabetes and beta cell function: from mechanisms to evaluation and clinical implications', *Biochem Med (Zagreb)*, 23: 266-80.

Chavhan, G.B., P.S. Babyn, B. Thomas, M.M. Shroff, and E.M. Haacke. 2009. 'Principles, techniques, and applications of T2*-based MR imaging and its special applications', *Radiographics*, 29: 1433-49.

Chen, K. Y., A. M. Cypess, M. R. Laughlin, C. R. Haft, H. H. Hu, M. A. Bredella, S. Enerback, P. E. Kinahan, Wv Lichtenbelt, F. I. Lin, J. J. Sunderland, K. A. Virtanen, and R. L. Wahl. 2016. 'Brown Adipose Reporting Criteria in Imaging Studies (BARCIST 1.0): Recommendations for Standardized FDG-PET/CT Experiments in Humans', *Cell Metab*, 24: 210-22.

Chen, Y.C., A.M. Cypess, Y.C. Chen, M. Palmer, G. Kolodny, C.R. Kahn, and K.K. Kwong. 2013. 'Measurement of human brown adipose tissue volume and activity using anatomic MR imaging and functional MR imaging', *J. Nucl. Med*, 54: 1584-87.

Chondronikola, M., E. Volpi, E. Borsheim, C. Porter, M. K. Saraf, P. Annamalai, C. Yfanti, T. Chao, D. Wong, K. Shinoda, S. M. Labbe, N. M. Hurren, F. Cesani, S. Kajimura, and L. S. Sidossis. 2016. 'Brown Adipose Tissue Activation Is Linked to Distinct Systemic Effects on Lipid Metabolism in Humans', *Cell Metab*, 23: 1200-06.

Cinti, S. 2006. 'The role of brown adipose tissue in human obesity', *Nutr. Metab Cardiovasc. Dis*, 16: 569-74.

Cinti, S. 2009. 'Transdifferentiation properties of adipocytes in the adipose organ', *Am. J. Physiol Endocrinol. Metab*, 297: E977-E86.

Cinti, S. 2011. 'Between brown and white: novel aspects of adipocyte differentiation', *Ann Med*, 43: 104-15.

Cinti, S. 2012. 'The adipose organ at a glance', *Dis. Model. Mech*, 5: 588-94.

Colberg, S.R., R.J. Sigal, B. Fernhall, J.G. Regensteiner, B.J. Blissmer, R.R. Rubin, L. Chasan-Taber, A.L. Albright, and B. Braun. 2010. 'Exercise and type 2 diabetes: the American College of Sports Medicine and the American Diabetes Association: joint position statement', *Diabetes Care*, 33: e147-e67.

Croteau, E., E. Lavallee, S. M. Labbe, L. Hubert, F. Pifferi, J. A. Rousseau, S. C. Cunnane, A. C. Carpentier, R. Lecomte, and F. Benard. 2010. 'Image-derived input function in dynamic human PET/CT: methodology and validation with 11C-acetate and 18F-fluorothioheptadecanoic acid in muscle and

18F-fluorodeoxyglucose in brain', *Eur J Nucl Med Mol Imaging*, 37: 1539-50.

Cypess, A.M., S. Lehman, G. Williams, I. Tal, D. Rodman, A.B. Goldfine, F.C. Kuo, E.L. Palmer, Y.H. Tseng, A. Doria, G.M. Kolodny, and C.R. Kahn. 2009. 'Identification and importance of brown adipose tissue in adult humans', *N. Engl. J. Med*, 360: 1509-17.

D'Agostino, R.B., Sr., R.S. Vasan, M.J. Pencina, P.A. Wolf, M. Cobain, J.M. Massaro, and W.B. Kannel. 2008. 'General cardiovascular risk profile for use in primary care: the Framingham Heart Study', *Circulation*, 117: 743-53.

da Rocha, Fernandes J., K. Ogurtsova, U. Linnenkamp, L. Guariguata, T. Seuring, P. Zhang, D. Cavan, and L.E. Makaroff. 2016. 'IDF Diabetes Atlas estimates of 2014 global health expenditures on diabetes', *Diabetes Res. Clin. Pract*, 117: 48-54.

Das, Birendra Kishore. 2015. Positron Emission Tomography - A Guide for Clinicians.

de Langen, A. J., V. E. van den Boogaart, J. T. Marcus, and M. Lubberink. 2008. 'Use of H2(15)O-PET and DCE-MRI to measure tumor blood flow', *Oncologist*, 13: 631-44.

DeFronzo, R.A., J.D. Tobin, and R. Andres. 1979. 'Glucose clamp technique: a method for quantifying insulin secretion and resistance', *Am. J Physiol*, 237: E214-E23.

Deng, J., L. M. Neff, N. C. Rubert, B. Zhang, R. M. Shore, J. D. Samet, P. C. Nelson, and L. Landsberg. 2017. 'MRI characterization of brown adipose tissue under thermal challenges in normal weight, overweight, and obese young men', *J Magn Reson Imaging*.

Deng, J., S.E. Schoeneman, H. Zhang, S. Kwon, C.K. Rigsby, R.M. Shore, and J.L. Josefson. 2015. 'MRI characterization of brown adipose tissue in obese and normal-weight children', *Pediatr. Radiol*, 45: 1682-89.

Din, U., J. Raiko, T. Saari, N. Kudomi, T. Tolvanen, V. Oikonen, J. Teuho, H.T. Sipila, N. Savisto, R. Parkkola, P. Nuutila, and K.A. Virtanen. 2016. 'Human brown adipose tissue [(15)O]O2 PET imaging in the presence and absence of cold stimulus', *Eur. J. Nucl. Med. Mol. Imaging*, 43: 1878-86.

Dixon, W.T. 1984. 'Simple proton spectroscopic imaging', *Radiology*, 153: 189-94.

Drubach, L.A., E.L. Palmer, III, L.P. Connolly, A. Baker, D. Zurakowski, and A.M. Cypess. 2011. 'Pediatric brown adipose tissue: detection, epidemiology, and differences from adults', *J. Pediatr*, 159: 939-44.

Dundamadappa, S.K., S. Shankar, R. Danrad, A. Singh, G. Vijayaraghavan, Y. Kim, and R. Perugini. 2007. 'Imaging of brown fat associated with adrenal pheochromocytoma', *Acta Radiol*, 48: 468-72.

Eggers, H., B. Brendel, A. Duijndam, and G. Herigault. 2011. 'Dual-echo Dixon imaging with flexible choice of echo times', *Magn Reson. Med*, 65: 96-107.

Emblem, K.E., K. Mouridsen, A. Bjornerud, C.T. Farrar, D. Jennings, R.J. Borra, P.Y. Wen, P. Ivy, T.T. Batchelor, B.R. Rosen, R.K. Jain, and A.G. Sorensen. 2013. 'Vessel architectural imaging identifies cancer patient responders to anti-angiogenic therapy', *Nat. Med*, 19: 1178-83.

Franssens, B.T., A.L. Eikendal, T. Leiner, Y. van der Graaf, F.L. Visseren, and J.M. Hoogduin. 2016. 'Reliability and agreement of adipose tissue fat fraction measurements with water-fat MRI in patients with manifest cardiovascular disease', *NMR Biomed*, 29: 48-56.

Franssens, B.T., H. Hoogduin, T. Leiner, Y. van der Graaf, and F.L. Visseren. 2017. 'Relation between brown adipose tissue and measures of obesity and metabolic dysfunction in patients with cardiovascular disease', *J Magn Reson. Imaging*.

Franz, D., D.C. Karampinos, E.J. Rummeny, M. Souvatzoglou, A.J. Beer, S.G. Nekolla, M. Schwaiger, and M. Eiber. 2015. 'Discrimination Between Brown and White Adipose Tissue Using a 2-Point Dixon Water-Fat Separation Method in Simultaneous PET/MRI', *J. Nucl. Med*, 56: 1742-47.

Green, A. L., U. Bagci, S. Hussein, P. V. Kelly, R. Muzaffar, B. A. Neuschwander-Tetri, and M. M. Osman. 2017. 'Brown adipose tissue detected by PET/CT imaging is associated with less central obesity', *Nucl Med Commun*, 38: 629-35.

Guilherme, A., J.V. Virbasius, V. Puri, and M.P. Czech. 2008. 'Adipocyte dysfunctions linking obesity to insulin resistance and type 2 diabetes', *Nat. Rev. Mol. Cell Biol*, 9: 367-77.

Hamdy, O., S. Porramatikul, and E. Al-Ozairi. 2006. 'Metabolic obesity: the paradox between visceral and subcutaneous fat', *Curr Diabetes Rev*, 2: 367-73.

Hamilton, M.T., D.G. Hamilton, and T.W. Zderic. 2014. 'Sedentary behavior as a mediator of type 2 diabetes', *Med. Sport Sci*, 60: 11-26.

Hausman, D. B., M. DiGirolamo, T. J. Bartness, G. J. Hausman, and R. J. Martin. 2001. 'The biology of white adipocyte proliferation', *Obes Rev*, 2: 239-54.

Hu, H. H., P. Bornert, D. Hernando, P. Kellman, J. Ma, S. Reeder, and C. Sirlin. 2012. 'ISMRM workshop on fat-water separation: insights, applications and progress in MRI', *Magn Reson Med*, 68: 378-88.

Hu, H.H., T.G. Perkins, J.M. Chia, and V. Gilsanz. 2013. 'Characterization of human brown adipose tissue by chemical-shift water-fat MRI', *AJR Am. J. Roentgenol*, 200: 177-83.

Hu, H.H., L. Yin, P.C. Aggabao, T.G. Perkins, J.M. Chia, and V. Gilsanz. 2013. 'Comparison of brown and white adipose tissues in infants and children with chemical-shift-encoded water-fat MRI', *J. Magn Reson. Imaging*, 38: 885-96.

IDF. 2015. 'IDF Diabetes Atlas, 7th edition', International Diabetes Federation. http://www.diabetesatlas.org.

Inokuma, K., Y. Ogura-Okamatsu, C. Toda, K. Kimura, H. Yamashita, and M. Saito. 2005. 'Uncoupling protein 1 is necessary for norepinephrine-induced glucose utilization in brown adipose tissue', *Diabetes*, 54: 1385-91.

Iwen, K. A., J. Backhaus, M. Cassens, M. Waltl, O. C. Hedesan, M. Merkel, J. Heeren, C. Sina, L. Rademacher, A. Windjager, A. R. Haug, F. W. Kiefer, H. Lehnert, and S. M. Schmid. 2017. 'Cold-induced brown adipose tissue activity alters plasma fatty acids and improves glucose metabolism in men', *J Clin Endocrinol Metab*.

Jang, C., S. Jalapu, M. Thuzar, P. W. Law, S. Jeavons, J. L. Barclay, and K. K. Ho. 2014. 'Infrared thermography in the detection of brown adipose tissue in humans', *Physiol Rep*, 2.

Jezek, P., and K.D. Garlid. 1998. 'Mammalian mitochondrial uncoupling proteins', *Int. J. Biochem. Cell Biol*, 30: 1163-68.

Karakatsanis, N. A., M. A. Lodge, A. K. Tahari, Y. Zhou, R. L. Wahl, and A. Rahmim. 2013. 'Dynamic whole-body PET parametric imaging: I. Concept, acquisition protocol optimization and clinical application', *Phys Med Biol*, 58: 7391-418.

Kato, K., T. Takamura, Y. Takeshita, Y. Ryu, H. Misu, T. Ota, K. Tokuyama, S. Nagasaka, M. Matsuhisa, O. Matsui, and S. Kaneko. 2014. 'Ectopic fat accumulation and distant organ-specific insulin resistance in Japanese people with nonalcoholic fatty liver disease', *PLoS. One*, 9: e92170.

Kern, P.A., S. Ranganathan, C. Li, L. Wood, and G. Ranganathan. 2001. 'Adipose tissue tumor necrosis factor and interleukin-6 expression in human obesity and insulin resistance', *Am. J. Physiol Endocrinol. Metab*, 280: E745-E51.

Kety, Seymour S., and Carl F. Schmidt. 1945. 'THE DETERMINATION OF CEREBRAL BLOOD FLOW IN MAN BY THE USE OF NITROUS OXIDE IN LOW CONCENTRATIONS', *American Journal of Physiology -- Legacy Content*, 143: 53.

Koksharova, E., D. Ustyuzhanin, Y. Philippov, A. Mayorov, M. Shestakova, M. Shariya, S. Ternovoy, and I. Dedov. 2017. 'The Relationship Between Brown Adipose Tissue Content in Supraclavicular Fat Depots and Insulin Sensitivity in Patients with Type 2 Diabetes Mellitus and Prediabetes', *Diabetes Technol Ther*, 19: 96-102.

Konig, M., E.M. Lamos, S.A. Stein, and S.N. Davis. 2013. 'An insight into the recent diabetes trials: what is the best approach to prevent macrovascular and microvascular complications?', *Curr. Diabetes Rev*, 9: 371-81.

Koskensalo, K., J. Raiko, T. Saari, V. Saunavaara, O. Eskola, P. Nuutila, J. Saunavaara, R. Parkkola, and K.A. Virtanen. 2017. 'Human Brown Adipose Tissue Temperature and Fat Fraction Are Related to Its Metabolic Activity', *J Clin. Endocrinol. Metab*, 102: 1200-07.

Lahesmaa, M., J. Orava, C. Schalin-Jantti, M. Soinio, J.C. Hannukainen, T. Noponen, A. Kirjavainen, H. Iida, N. Kudomi, S. Enerback, K.A. Virtanen, and P. Nuutila. 2014. 'Hyperthyroidism increases brown fat metabolism in humans', *J. Clin. Endocrinol. Metab*, 99: E28-E35.

Lee, P., J.R. Greenfield, K.K. Ho, and M.J. Fulham. 2010. 'A critical appraisal of the prevalence and metabolic significance of brown adipose tissue in adult humans', *Am. J. Physiol Endocrinol. Metab*, 299: E601-E06.

Leitner, B. P., S. Huang, R. J. Brychta, C. J. Duckworth, A. S. Baskin, S. McGehee, I. Tal, W. Dieckmann, G. Gupta, G. M. Kolodny, K. Pacak, P. Herscovitch, A. M. Cypess, and K. Y. Chen. 2017. 'Mapping of human brown adipose tissue in lean and obese young men', *Proc Natl Acad Sci U S A*, 114: 8649-54.

Lidell, M.E., M.J. Betz, Leinhard O. Dahlqvist, M. Heglind, L. Elander, M. Slawik, T. Mussack, D. Nilsson, T. Romu, P. Nuutila, K.A. Virtanen, F. Beuschlein, A. Persson, M. Borga, and S. Enerback. 2013. 'Evidence for two types of brown adipose tissue in humans', *Nat. Med*, 19: 631-34.

Loh, R. K. C., B. A. Kingwell, and A. L. Carey. 2017. 'Human brown adipose tissue as a target for obesity management; beyond cold-induced thermogenesis', *Obes Rev*.

Lunati, E., P. Marzola, E. Nicolato, M. Fedrigo, M. Villa, and A. Sbarbati. 1999. 'In vivo quantitative lipidic map of brown adipose tissue by chemical shift imaging at 4.7 Tesla', *J. Lipid Res*, 40: 1395-400.

Lundbom, J., A. Hakkarainen, B. Fielding, S. Soderlund, J. Westerbacka, M.R. Taskinen, and N. Lundbom. 2010. 'Characterizing human adipose tissue lipids by long echo time 1H-MRS in vivo at 1.5 Tesla: validation by gas chromatography', *NMR Biomed*, 23: 466-72.

Lundstrom, E., R. Strand, L. Johansson, P. Bergsten, H. Ahlstrom, and J. Kullberg. 2015. 'Magnetic resonance imaging cooling-reheating protocol indicates decreased fat fraction via lipid consumption in suspected brown adipose tissue', *PLoS. One*, 10: e0126705.

Ma, J. 2008. 'Dixon techniques for water and fat imaging', *J. Magn Reson. Imaging*, 28: 543-58.

Marette, A. 2003. 'Molecular mechanisms of inflammation in obesity-linked insulin resistance', *Int. J. Obes. Relat Metab Disord*, 27 Suppl 3: S46-S48.

Matsushita, M., T. Yoneshiro, S. Aita, T. Kameya, H. Sugie, and M. Saito. 2014. 'Impact of brown adipose tissue on body fatness and glucose metabolism in healthy humans', *Int. J Obes. (Lond)*, 38: 812-17.

McCulloch, M., C. Gresser, S. Moos, J. Odabashian, S. Jasper, J. Bednarz, P. Burgess, D. Carney, V. Moore, E. Sisk, A. Waggoner, S. Witt, and D. Adams. 2000. 'Ultrasound contrast physics: A series on contrast echocardiography, article 3', *J Am Soc Echocardiogr*, 13: 959-67.

Mokdad, A.H., E.S. Ford, B.A. Bowman, W.H. Dietz, F. Vinicor, V.S. Bales, and J.S. Marks. 2003. 'Prevalence of obesity, diabetes, and obesity-related health risk factors, 2001', *JAMA*, 289: 76-79.

Moller, D. E., and K. D. Kaufman. 2005. 'Metabolic syndrome: a clinical and molecular perspective', *Annu Rev Med*, 56: 45-62.

Montague, C.T., and S. O'Rahilly. 2000. 'The perils of portliness: causes and consequences of visceral adiposity', *Diabetes*, 49: 883-88.

Nedergaard, J., T. Bengtsson, and B. Cannon. 2007. 'Unexpected evidence for active brown adipose tissue in adult humans', *Am. J. Physiol Endocrinol. Metab*, 293: E444-E52.

Ojanen, X., R.J. Borra, M. Havu, S.M. Cheng, R. Parkkola, P. Nuutila, M. Alen, and S. Cheng. 2014. 'Comparison of vertebral bone marrow fat assessed by 1H MRS and inphase and out-of-phase MRI among family members', *Osteoporos. Int*, 25: 653-62.

Okorodudu, D. O., M. F. Jumean, V. M. Montori, A. Romero-Corral, V. K. Somers, P. J. Erwin, and F. Lopez-Jimenez. 2010. 'Diagnostic performance of body mass index to identify obesity as defined by body adiposity: a systematic review and meta-analysis', *Int J Obes (Lond)*, 34: 791-9.

Orava, J., P. Nuutila, M.E. Lidell, V. Oikonen, T. Noponen, T. Viljanen, M. Scheinin, M. Taittonen, T. Niemi, S. Enerback, and K.A. Virtanen. 2011. 'Different metabolic responses of human brown adipose tissue to activation by cold and insulin', *Cell Metab*, 14: 272-79.

Orava, J., P. Nuutila, T. Noponen, R. Parkkola, T. Viljanen, S. Enerback, A. Rissanen, K.H. Pietilainen, and K.A. Virtanen. 2013. 'Blunted metabolic responses to cold and insulin stimulation in brown adipose tissue of obese humans', *Obesity. (Silver. Spring)*.

Ouellet, V., A. Routhier-Labadie, W. Bellemare, L. Lakhal-Chaieb, E. Turcotte, A.C. Carpentier, and D. Richard. 2011. 'Outdoor temperature, age, sex, body mass index, and diabetic status determine the prevalence, mass, and glucose-uptake activity of 18F-FDG-detected BAT in humans', *J Clin. Endocrinol. Metab*, 96: 192-99.

Pooley, R.A. 2005. 'AAPM/RSNA physics tutorial for residents: fundamental physics of MR imaging', *Radiographics*, 25: 1087-99.

Porter, D.A., and R.M. Heidemann. 2009. 'High resolution diffusion-weighted imaging using readout-segmented echo-planar imaging, parallel imaging and a two-dimensional navigator-based reacquisition', *Magn Reson. Med*, 62: 468-75.

Provencher, S.W. 2001. 'Automatic quantitation of localized in vivo 1H spectra with LCModel', *NMR Biomed*, 14: 260-64.

Purcell, E.M. 1945. 'Resonance Absorption by Nuclear Magnetic Moments in a Solid'.

Quinn, B., Z. Dauer, N. Pandit-Taskar, H. Schoder, and L.T. Dauer. 2016. 'Radiation dosimetry of 18F-FDG PET/CT: incorporating exam-specific parameters in dose estimates', *BMC. Med. Imaging*, 16: 41.

Reeder, S. B., I. Cruite, G. Hamilton, and C. B. Sirlin. 2011. 'Quantitative assessment of liver fat with magnetic resonance imaging and spectroscopy', *J Magn Reson Imaging*, 34: 729-49.

Romu, T., L. Elander, O.D. Leinhard, M.E. Lidell, M.J. Betz, A. Persson, S. Enerback, and M. Borga. 2015. 'Characterization of brown adipose tissue by water-fat separated magnetic resonance imaging', *J. Magn Reson. Imaging*, 42: 1639-45.

Rosenwald, M., A. Perdikari, T. Rulicke, and C. Wolfrum. 2013. 'Bi-directional interconversion of brite and white adipocytes', *Nat. Cell Biol*, 15: 659-67.

Saito, M., Y. Okamatsu-Ogura, M. Matsushita, K. Watanabe, T. Yoneshiro, J. Nio-Kobayashi, T. Iwanaga, M. Miyagawa, T. Kameya, K. Nakada, Y. Kawai, and M. Tsujisaki. 2009. 'High incidence of metabolically active brown adipose tissue in healthy adult humans: effects of cold exposure and adiposity', *Diabetes*, 58: 1526-31.

Sattar, N., and J. M. Gill. 2014. 'Type 2 diabetes as a disease of ectopic fat?', *BMC Med*, 12: 123.

Sbarbati, A., U. Guerrini, P. Marzola, R. Asperio, and F. Osculati. 1997. 'Chemical shift imaging at 4.7 tesla of brown adipose tissue', *J. Lipid Res*, 38: 343-47.

Schenck, J.F. 1996. 'The role of magnetic susceptibility in magnetic resonance imaging: MRI magnetic compatibility of the first and second kinds', *Med. Phys*, 23: 815-50.

Schrover, I.M., T. Leiner, D.W. Klomp, J.P. Wijnen, C.S. Uiterwaal, W. Spiering, and F.L. Visseren. 2014. 'Feasibility and reproducibility of free fatty acid profiling in abdominal adipose tissue with 1H-magnetic resonance spectroscopy at 3 T: differences between lean and obese individuals', *J. Magn Reson. Imaging*, 40: 423-31.

Scotney, H., M.E. Symonds, J. Law, H. Budge, D. Sharkey, and K.N. Manolopoulos. 2017. 'Glucocorticoids modulate human brown adipose tissue thermogenesis in vivo', *Metabolism*, 70: 125-32.

Seo, M., J.K. Ryu, G.H. Jahng, Y.M. Sohn, S.J. Rhee, J.H. Oh, and K.Y. Won. 2017. 'Estimation of T2* Relaxation Time of Breast Cancer: Correlation with Clinical, Imaging and Pathological Features', *Korean J. Radiol*, 18: 238-48.

Sharp, P.F. 1994. 'The measurement of blood flow in humans using radioactive tracers', *Physiol Meas*, 15: 339-79.

Shaw, J.E., R.A. Sicree, and P.Z. Zimmet. 2010. 'Global estimates of the prevalence of diabetes for 2010 and 2030', *Diabetes Res. Clin. Pract*, 87: 4-14.

Siemens. 2009. 'MR Glossary'.

Sipilä, H.T, J.C Clark, O Peltola, and M Teräs. 2001. 'An automatic [15O]H2O production system for heart and brain studies.', *J Label Compd Radiopharm*, 44: s1066-s68.

Sokoloff, L., M. Reivich, C. Kennedy, M.H. Des Rosiers, C.S. Patlak, K.D. Pettigrew, O. Sakurada, and M. Shinohara. 1977. 'The [14C]deoxyglucose method for the measurement of local cerebral glucose utilization: theory, procedure, and normal values in the conscious and anesthetized albino rat', *J. Neurochem*, 28: 897-916.

Stahl, V., F. Maier, M.T. Freitag, R.O. Floca, M.C. Berger, R. Umathum, Diaz M. Berriel, S. Herzig, M.A. Weber, A. Dimitrakopoulou-Strauss, K. Rink, P. Bachert, M.E. Ladd, and A.M. Nagel. 2016. 'In vivo assessment of cold stimulation effects on the fat fraction of brown adipose tissue using DIXON MRI', *J. Magn Reson. Imaging*.

Sun, L., J. Yan, L. Sun, S.S. Velan, and M.K.S. Leow. 2017. 'A synopsis of brown adipose tissue imaging modalities for clinical research', *Diabetes Metab*.

Tanaka, S., M. Yoshiyama, Y. Imanishi, M. Teragaki, N. Kasayuki, N. Shimizu, K. Nakahira, T. Hanaki, Y. Naito, M. Tanaka, and Y. Inoue. 2007. 'Measuring visceral fat with water-selective suppression methods (SPIR, SPAIR) in patients with metabolic syndrome', *Magn Reson. Med. Sci*, 6: 171-75.

Turner, R. 1993. 'Gradient coil design: a review of methods', *Magn Reson Imaging*, 11: 903-20.

van Marken Lichtenbelt, W.D., J.W. Vanhommerig, N.M. Smulders, J.M. Drossaerts, G.J. Kemerink, N.D. Bouvy, P. Schrauwen, and G.J. Teule. 2009. 'Cold-activated brown adipose tissue in healthy men', *N. Engl. J. Med*, 360: 1500-08.

van Rooijen, B.D., A.A. van der Lans, B. Brans, J.E. Wildberger, F.M. Mottaghy, P. Schrauwen, W.H. Backes, and W.D. van Marken Lichtenbelt. 2013. 'Imaging cold-activated brown adipose tissue using dynamic T2*-weighted magnetic resonance imaging and 2-deoxy-2-[18F]fluoro-D-glucose positron emission tomography', *Invest Radiol*, 48: 708-14.

Virtanen, K.A., M.E. Lidell, J. Orava, M. Heglind, R. Westergren, T. Niemi, M. Taittonen, J. Laine, N.J. Savisto, S. Enerback, and P. Nuutila. 2009. 'Functional brown adipose tissue in healthy adults', *N. Engl. J. Med*, 360: 1518-25.

WHO. 2013. 'WHO Global Strategy on Diet, Physical Activity and Health', WHO. http://www.who.int/dietphysicalactivity/strategy/en/.

WHO. 2016. 'Global report on diabetes'. http://www.who.int/diabetes/global-report/en/.

Willowson, K.P., E.A. Bailey, and D.L. Bailey. 2012. 'A retrospective evaluation of radiation dose associated with low dose FDG protocols in whole-body PET/CT', *Australas. Phys. Eng Sci. Med*, 35: 49-53.

Wilson, P.W., J.B. Meigs, L. Sullivan, C.S. Fox, D.M. Nathan, and R.B. D'Agostino, Sr. 2007. 'Prediction of incident diabetes mellitus in middle-aged adults: the Framingham Offspring Study', *Arch. Intern. Med*, 167: 1068-74.

Wu, J., P. Bostrom, L.M. Sparks, L. Ye, J.H. Choi, A.H. Giang, M. Khandekar, K.A. Virtanen, P. Nuutila, G. Schaart, K. Huang, H. Tu, W.D. van Marken Lichtenbelt, J. Hoeks, S. Enerback, P. Schrauwen, and B.M. Spiegelman. 2012. 'Beige adipocytes are a distinct type of thermogenic fat cell in mouse and human', *Cell*, 150: 366-76.

Yoneshiro, T., S. Aita, M. Matsushita, Y. Okamatsu-Ogura, T. Kameya, Y. Kawai, M. Miyagawa, M. Tsujisaki, and M. Saito. 2011. 'Age-related decrease in cold-activated brown adipose tissue and accumulation of body fat in healthy humans', *Obesity. (Silver. Spring)*, 19: 1755-60.

Annales Universitatis Turkuensis

Turun yliopisto
University of Turku

ISBN 978-951-29-7187-9 (PRINT)
ISBN 978-951-29-7188-6 (PDF)
ISSN 0355-9483 (Print) | ISSN 2343-3213 (Online)

Painosalama Oy, Turku, Finland 2018